UNDERSTANDING THE ACTIVATION OF BACTERIAL PROTEASE CLPP BY ACYLDEPSIPEPTIDE ANTIBIOTIC

BY: **BILAL AHSAN, B.Sc**

A Thesis Submitted to the School of Graduate Studies In Partial Fulfillment of the Requirements for the Degree Master of Science

MASTER OF SCIENCE (2014)

McMaster University (Biochemistry and Biomedical Sciences) Hamilton, Ontario

TITLE: Understanding the activation of bacterial protease ClpP by acyldepsipeptide antibiotic.

AUTHOR: Bilal Ahsan (McMaster University)

SUPERVISOR: Dr. Joaquin Ortega

NUMBER OF PAGES: viii,75

ABSTRACT

Acyldepsipeptide (ADEP1) is an antibiotic that binds to *Escherichia coli* ClpP, mimicking the interaction that the protease typically establishes with ClpA/ClpX ATPases in bacterial cells. Binding of ADEP1 causes the N-terminal end of the ClpP to adopt a structured β-hairpin and triggers opening of the axial gate in the tetradecameric ClpP. Open conformation of the axial gate causes translocation of the substrates into the catalytic chamber of ClpP and the resultant uncontrolled proteolysis renders cellular death making ADEP1 a potent antibiotic. Our current understanding about the ADEP1-induced open conformation of the axial gate is limited. Based on the existing X-ray structures, it is unclear whether the mechanism of ADEP1-mediated activation of ClpP is conserved in Gram-positive and Gram-negative bacteria. To understand the activation mechanism of ClpP by ADEP1, we obtained *Bacillus subtilis* ClpP variants with amino acid substitutions in the N-terminal region and tested the effect of these mutations on substrate translocation using fluorescence-based proteolytic assays and cryo-electron microscopy. We found that compromising the integrity of the β-hairpin adopted by the N-terminal region prevented translocation of the substrate into the catalytic chamber of *B. subtilis* ClpP. These results suggest that the structural requirements for a functional axial channel are conserved in Gram-positive and Gram-negative bacteria. This study defines the structural requirements for ADEP1-mediated activation of the ClpP protease and serves as a model for the functioning of ClpP in the context of the ClpAP and ClpXP complexes.

ACKNOWLEDGEMENTS

First, I would like to express my sincerest gratitude to my supervisor Dr. Joaquin Ortega for giving me the opportunity to experience the amazing world of scientific research. You have allowed me to continue my passion for science and instilled values in me that I will carry into my future career. You have not only supervised me in research, but also academically and emotionally during the completion of my degree. I would also like to thank my committee members Dr. Alba Guarné and Dr. Lori Burrows for their valuable guidance. In addition I would like to thank members of the Ortega lab, past and present, especially Brett Thurlow and Dr. Ahmad Jomaa for helpful discussions. Thanks to Vivian Leong for providing me with the technical assistance necessary for investigating my research objectives. I would like to thank Dr. Richard M. Epand and for letting me use the instruments to conduct my ITC experiments.

I would like to thank Hafiz Sohail Naushad for his friendship and moral support. You have always helped me to successfully face the challenges in my personal and academic life.

I would like to express a very special thanks to my mother, and siblings who provide me unconditional love and support. Finally, to my wife and daughter Muqaddas, thanks for two years of sacrifice and allowing me to follow my ambition. Without you, I most certainly would not be where I am today. Although you were thousands of miles away, you have been my strength and motivation throughout my graduate studies. Words cannot express how much I love you and how grateful I am for your support.

Table of Contents

LIST OF TABLES AND FIGURES

LIST OF ABBREVIATIONS

A_{230}	light absorbance at 230 nanometers (wavelength)
AAA+	ATPases associated with various cellular activities
ADEP	acyldepsipeptide
ATP	adenosine triphosphate
ATPase	adenosine triphosphatase
ATPγS	adenosine 5' (gamma-thio) triphosphate
*Bs*ClpP	*Bacillus subtilis* ClpP
ClpA	caseinolytic Protease A
ClpP	caseinolytic Protease P
ClpX	caseinolytic Protease X
Cryo-EM	Cryo electron microscopy
DMSO	dimethyl sulfoxide
DNA	deoxyribonucleic acid
DTT	dithiothreitol
*Ec*ClpP	*Escherichia coli* ClpP
IPTG	Isoproply β-D-1-thiogalactopyranoside
ITC	Isothermal titration calorimetry
k_{cat}	constant that describes the turnover rate of an enzyme-substrate complex to the product and enzyme
K_m	Michaelis constant that describes the amount of substrate needed for the enzyme to obtain half of its maximum rate of reaction
OD_{600}	Optical density of light at wavelength 600 nanometer
PDB	protein data bank
SDS-PAGE	sodium dodecyl-sulfate polyacrylamide gel electrophoresis
*Sh*ClpP	*Streptomyces hawaiiensis* ClpP

1. Introduction

1.1 Proteolysis in bacteria

Energy dependent proteolysis is a fundamental process in bacteria where defective and misfolded proteins are degraded to prevent detrimental aggregation (Sauer *et al.* 2004). Five distinct classes of proteases known as ClpAP, ClpXP, FtsH, Lon, and HsIUV carry out regulated proteolysis in Gram-negative bacteria (Langklotz, Baumann and Narberhaus 2011). Additional proteases called ClpEP and ClpCP are also found in several Gram-positive bacteria (Gur, Biran and Ron 2011). Among these proteases, caseinolytic protease P (ClpP) is highly conserved in prokaryotes and carries out most of the cellular protein degradation. Substrate trapping pull down assays indicate that ClpP degrades a variety of substrates including proteins associated with cell division, motility, translation and transcription (Feng *et al.* 2012, Flynn *et al.* 2003). ClpP is also implicated as an important regulator of cellular growth, virulence, and tolerance under heat shock in different organisms (Nair *et al.* 2003, Yu *et al.* 2007).

1.2 Architectural features of ClpP

The X-ray structures of ClpP from prokaryotes and eukaryotic mitochondria reveal highly conserved architectural features. The structure of the ClpP protomer is divided into the N-terminal loops, a globular region, and a handle domain (Figure 1A). Fourteen monomers of ClpP oligomerize as two heptameric rings that stack back to back to form a barrel-shaped tetradecamer

that encloses a catalytic chamber containing the fourteen catalytic sites (Figure 1B-C) (Bewley *et al.* 2006, Wang *et al.* 1997).

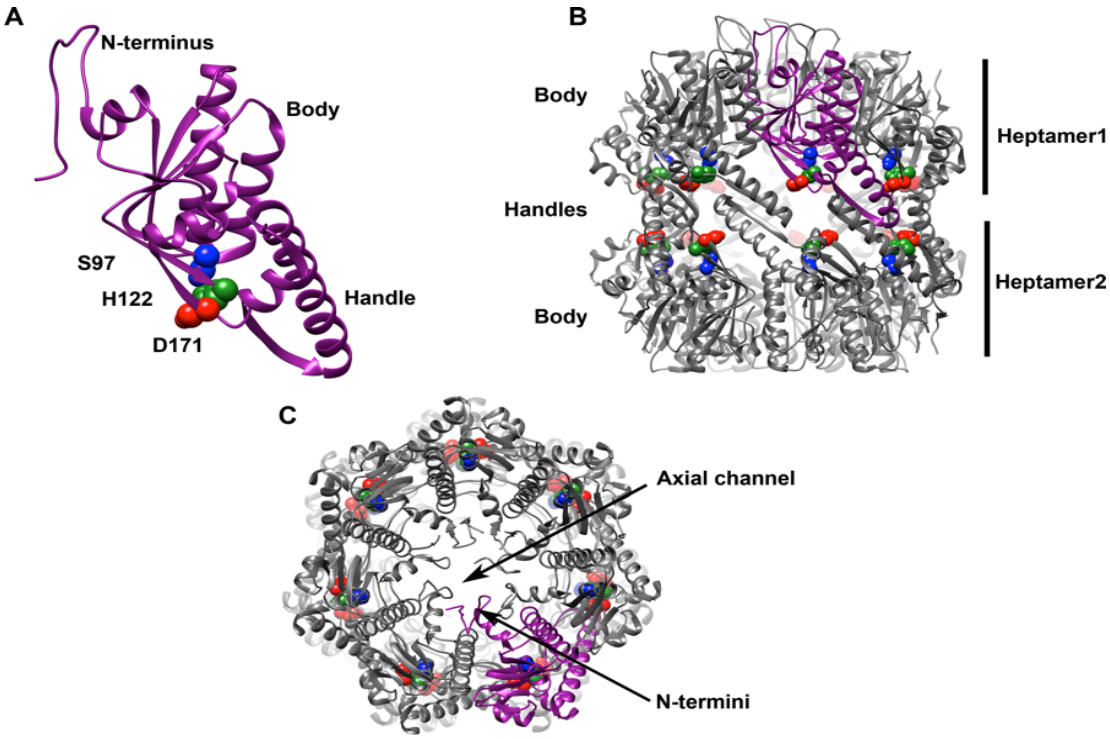

Figure 1: Architectural features of *E. coli* ClpP. Different structural views of X-ray structure of wild type *E. coli* ClpP (PDB 1YG6). **A**. One monomer of ClpP indicating the landmarks of N-terminus, body, and handle region. The catalytic residues of Ser97, His122 and Asp171 are shown in blue, green and red spheres respectively. **B**. Side-view of ClpP tetradecamer. Handle regions of two identical heptamers stack back to back to form a catalytic chamber of ClpP tetradecamer. One monomer is shown in magenta color for differentiation and the catalytic residues are colored same as in panel **A**. **C**. Top-view of ClpP tetradecamer showing the formation of axial channel gated by N-terminal residues.

1.3 Activation of ClpP by ATPase; ClpX/ClpA

In *E. coli* ClpP, the substrate access to the degradation chamber occurs through the axial pores, gated by the N-terminal region (Lee *et al.* 2010). Short peptides can diffuse through the axial pores, however passage of large

substrates requires the ATPases; ClpA/ClpX (Grimaud *et al.* 1998, Kessel *et al.* 1995, Thompson, Singh and Maurizi 1994, Wang, Hartling and Flanagan 1997). Biochemical studies, X-ray crystallography, (Bewley *et al.* 2006, Martin, Baker and Sauer 2007, Wang *et al.* 1997) and cryo-EM (Beuron *et al.* 1998, Grimaud *et al.* 1998, Effantin *et al.* 2010a) have established that ClpA/ClpX bind coaxially to the hydrophobic pockets at the outer edge of the ClpP oligomeric rings. This binding is mediated through the conserved tri-peptide, IGL or IGF in ClpA and ClpX respectively (Kim *et al.* 2001, Singh *et al.* 2001). Another, relatively weaker interaction between the pore 2 loops of ClpX and the N-termini of ClpP also contributes to communicate and regulate the activity of ClpP (Bewley *et al.* 2006, Martin *et al.* 2007).

Several studies have established that ATPases unfold and subsequently translocate the protein substrates into the catalytic chamber of ClpP by an ATP driven mechanism (Baker and Sauer 2006, Ishikawa *et al.* 2001, Ortega *et al.* 2000). However, the exact mechanism and the residues important to stabilize the open and closed conformation of the gate are still unknown. Variability of ClpX/A to form 1:1 and 2:1 complexes with ClpP and the symmetry mismatch (hexameric ATPase : heptameric ClpP) has hindered the generation of a high resolution 3 D structures of ClpX/A-ClpP by X-ray crystallography and single particle analysis of cryo-EM (Alexopoulos, Guarne and Ortega 2012, Effantin, Maurizi and Steven 2010b). Available structures of ClpX/A-ClpP complex are either low resolution 2D (Kessel *et al.* 1995, Ortega *et al.* 2000, Singh *et al.* 2001) composite 3 D (Beuron

et al. 1998), or low resolution 3D (Effantin *et al.* 2010b). Such structures do not provide a clear picture of the ATPase-ClpP interface (Alexopoulos *et al.* 2012). Therefore, the structural determinants required to stabilize the N-termini in the open conformation are still unknown.

1.4 ADEP1-induced axial gate opening models of ClpP

Recently, an atomic resolution crystal structure of EcClpP in complex with acyldepsipeptide (ADEP1) antibiotic (Li et al. 2010) was published providing the details of the open conformation of the axial gate. ADEP1 is a new class of antibiotic that binds to the same hydrophobic pockets present in the axial region of ClpP where IGF/L loops of ATPase bind (Figure 2A) (Lee et al. 2010a, Li et al. 2010). The mimicking interaction of ADEP1 with ClpP bypasses the requirement for ClpX or ClpA and deregulates the protease activity of ClpP. The resulting uncontrolled proteolysis of nascent peptides leads to cell death (Brotz-Oesterhelt et al. 2005, Kirstein et al. 2009). Binding of ADEP1 causes the N-termini of ClpP protomers to adopt a structured β-hairpin, which is stabilized by intra and intermolecular electrostatic interactions among four charged residues. First, the intramolecular interaction of Glu8 with the side-chain of Lys25 retracts the β-hairpin from the axial lumen and locks its orientation relative to the head domain of ClpP (Figure 2B). Second, the intermolecular interaction between Glu14 and Arg15 of the adjacent protomer staples the N-terminal loops and generates a defined rim of the axial gate (Figure 2C). Consequently, a structured axial gate of 20 Å in diameter appears in the axial region that is sufficient for the translocation of unfolded peptides into the catalytic chamber of ClpP (Li *et al.* 2010).

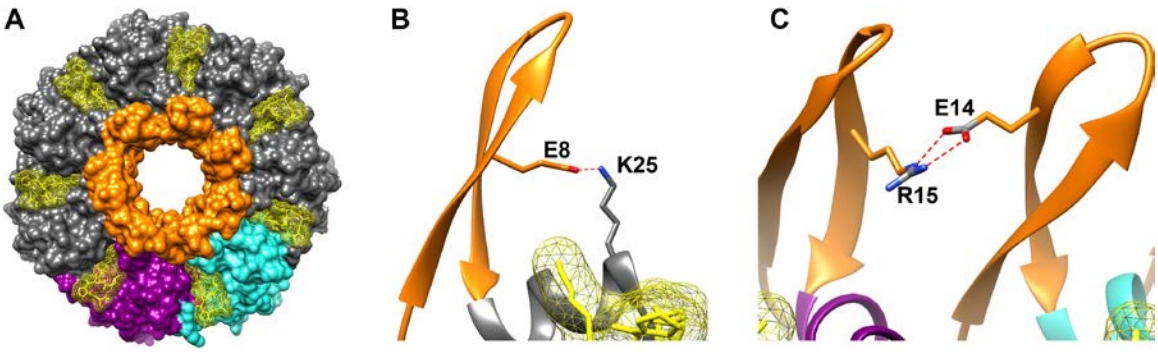

Figure 2: Crystal structure of ClpP in complex with ADEP1. A. Surface representation of the top-view of the crystal structure of *E. coli* ClpP tetradecamer in complex with ADEP1 (PDB 3MT6). Two monomers of ClpP are colored in magenta and cyan. The ADEP1 is represented as yellow contours bound in the hydrophobic pockets existing between adjacent monomers. The first 18 N-terminal residues shown in orange are lining the axial pore of 20 Å. **B**. N-terminal region of the ClpP protomer shown to adopt a structured β-hairpin (orange color) upon ADEP1 binding. Important residues involved in the intramolecular interactions contributing to the open conformation of the axial channel are highlighted. **C**. Residues involved in the intermolecular interactions of two adjacent protomers of *E. coli* ClpP.

The ADEP1 bound X-ray structure of *B. subtilis* ClpP, published in another study (Lee *et al.* 2010a) also shows that ADEP1 binds to the hydrophobic pockets of ClpP and opens the axial gate (Figure 3A). However, a different mechanism for the ADEP1-induced axial gate opening of ClpP is proposed in that study (Lee *et al.* 2010a). According to their model, side chains of Pro4, Val6 and Ilel19 of each ClpP monomer interact with the side chains of Leu24 and Phe49 of the adjoining monomer to form a hydrophobic cluster in free *Bs*ClpP (Figure 3B).

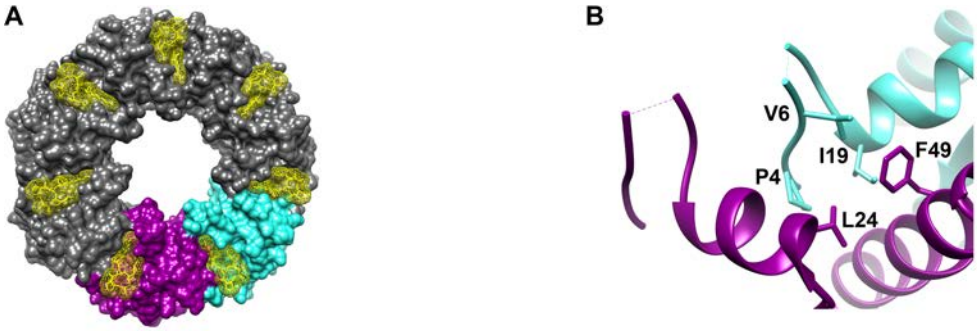

Figure 3: ADEP1-induced activation of ClpP in *B. subtilis.* A. Surface representation of the top-view of the crystal structure of *B. subtilis* ClpP in complex with ADEP1 (PDB 3KTI). Two monomers and ADEP1 molecules are colored the same as in A. N-terminal residues are not visible in this structure that results in opening of an axial pore of 27 Å. B. Interface of N-terminal regions of two adjacent monomers of free *Bs*ClpP with hydrophobic cluster region formed by the indicated residues (PDB 3KTG).

In the absence of ADEP1, this cluster region stabilizes each N-terminus of the ClpP monomers into a closed conformation of the axial gate. However, binding of ADEP1 triggers a structural change in *Bs*ClpP that is transmitted to the hydrophobic cluster region. Consequently, stabilizing interactions among the side chains of the residues contributing to the integrity of the hydrophobic cluster are compromised. Loss of stabilizing interactions introduces more flexibility in the N-terminal regions to generate pores of 27 Å on both axial regions of ClpP (Lee *et al.* 2010a). The authors attribute the flexible nature of the N-termini of ClpP to be the reason for not being visible in the crystal structure.

The controversy of the “structured” versus “unstructured” mechanism of axial gate opening of ClpP as proposed by the studies in *E. coli* (Li *et al.* 2010) and *B. subtilis* (Lee *et al.* 2010a) is unresolved. An extensive review on the structural comparison of *E. coli* and *B. subtilis* ClpP in complex with ADEP1

reveals that the observed conformation of a structured β-hairpin adopted by the N-terminal residues in the X-ray structure of *Ec*ClpP is not due to the artifact of crystal packing (Alexopoulos *et al.* 2012). In contrast, the apical surfaces of *Bs*ClpP structure show multiple crystal contacts with the adjacent tetradecamer. It is possible that the tight packing in the crystal structure of *Bs*ClpP prevented the N-terminal residues from adopting a structured β-hairpin. In addition, critical analysis of the hydrophobic cluster region shows its presence in the structures of free and ADEP1 bound ClpP of *E. coli* and *B. subtilis.* Therefore, the increased flexibility in the N-terminal region of *Bs*ClpP might be a consequence of crystal packing rather than disruption of the hydrophobic cluster due to ADEP1 binding (Alexopoulos *et al.* 2012). There are no experimental data to rule out the likelihood of a dissimilar mechanism involved in the open conformation of the axial gate of ClpP in *E. coli* and *B. subtilis* (Alexopoulos *et al.* 2012). Nonetheless, these studies provide the initial framework to investigate the structural determinants contributing towards the opening of axial pores upon ADEP1 binding and to ascertain if they hold the same architectural significance in Gram positive and in Gram negative bacteria.

1.5 Release of degradation products from the catalytic chamber of ClpP

Biochemical studies have shown that the substrates translocated into the catalytic chamber of ClpP are processively cleaved into fragments of seven to eight residues (Choi and Licht 2005, Licht and Lee 2008). However, the pathway of product release from the degradation chamber of ClpP is still under

investigation. It is proposed that the degradation products might exit the catalytic chamber of ClpP through the axial pore (Thompson and Maurizi 1994, Thompson *et al.* 1994). This proposal is backed by structural studies that suggest the possibility of product release from one of the two axial pores in 1:1 or continuously dissociating and re-associating 2:1 ClpX/AP complexes (Ortega *et al.* 2000, Ortega *et al.* 2004). This model is still up for debate, as utilizing the axial pore for product release would interrupt the translocation of the substrate into the catalytic chamber of the protease (Sprangers *et al.* 2005). A newly emerging model proposes that the degradation products are extruded through dynamically-formed side pores in the vicinity of the equatorial region and that the catalytic activity of ClpP is halted during the course of product release (Gribun *et al.* 2005, Sprangers *et al.* 2005, Lee, Kim and Song 2011).

Most of the available crystal structures of ClpP from different organisms show virtually no product exit site except for the axial pores. These structures are referred to as the “extended” form of ClpP (Figure 4A). In contrast, recently published X-ray structures of *Staphylococcus aureus* and *Bacillus subtilis* ClpP show a “compressed” state (Figure 4B) of ClpP with the presence of side pores in the equatorial region (Geiger *et al.* 2011, Lee *et al.* 2011). The secondary and tertiary elements of the “extended” and axially “compressed” forms of ClpP are very similar, even among X-ray structures from different species (Lee *et al.* 2011). However, there are noticeable differences observed for the handle region

in the different conformations of ClpP. Specifically, helix αE in the compressed structure of *S. aureus* ClpP is kinked and B6 is distorted (Figure 4C).

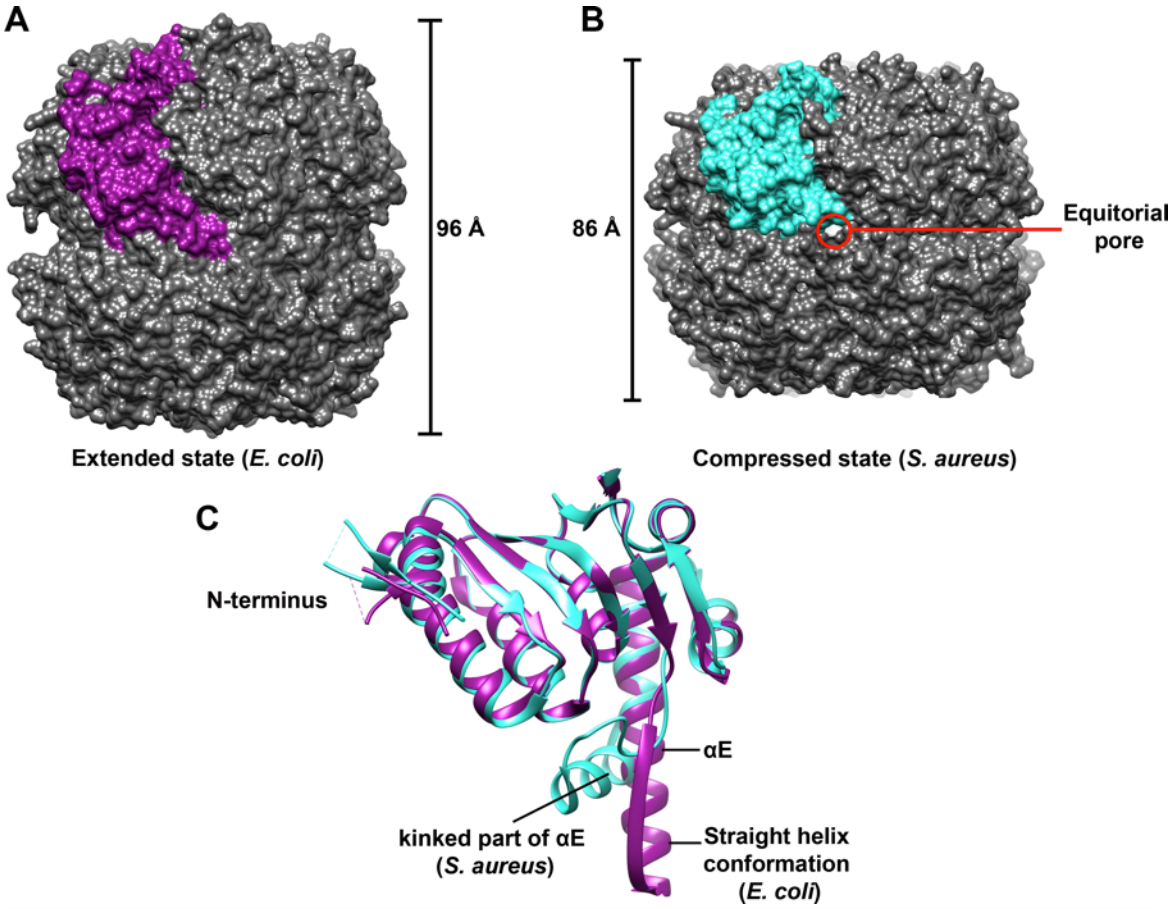

Figure 4: Extended and compressed states of ClpP. Surface representation of side views of the X-ray structures of *E. coli* ClpP (PDB 2FZS) in extended **(A)** and *S. aureus* ClpP (PDB 3QWD) in axially compressed state **(B)**. One monomer of ClpP in each of the tetradecamer is colored in magenta (*E. coli* ClpP) and cyan (*S. aureus* ClpP). The presence of the equatorial pore in the X-ray structure of *S. aureus* ClpP **(B)** is shown in the red circle. **C.** Overlap of the colored monomers shown in **A** and **B** with indicated differences in the handle region.

The conformation of the compressed state of ClpP confers a nonfunctional arrangement of the catalytic triad and disrupts the salt bridge observed between Glu135 and Arg171 of the adjacent monomer of ClpP. This salt bridge is

suggested as an important molecular interaction required for stabilizing the extended state of ClpP because its disruption leads to a compressed state. The characteristic features of a catalytically inactive protease with side pores in the equatorial region of compressed ClpP are attributed to a state that explains the pathway of product release (Geiger *et al.* 2011, Lee *et al.* 2011). Biochemical assays complement these structural findings and extrapolate previous NMR observations (Sprangers *et al.* 2005).

The X-ray structures of the extended (Wang *et al.* 1997, Bewley *et al.* 2006) and compressed states of ClpP (Geiger *et al.* 2011, Lee *et al.* 2011), biochemical (Geiger *et al.* 2011) and NMR studies (Sprangers *et al.* 2005) converge at a two-state "extended-compressed" model to explain processive ClpP protease function. According to this model, ATPase-activated ClpP degrades a substrate in its extended form. Fragments of the degraded substrate trigger a conformational change and ClpP moves into a catalytically inactive compressed state that reveals side pores for product release, and the cycle continues (Geiger *et al.* 2011). In the X-ray structure of the compressed state of *Bs*ClpP, the loop between αE and β6 in the handle region loop is highly disordered, with partial distortion of helix αE, presumably due to flexibility in this region (Lee *et al.* 2011). Additionally, the higher B-factor values (indicative of high flexibility) of these secondary structural elements in the crystal structure of *Sa*ClpP suggest that the equatorial region of ClpP in compressed state is flexible (Geiger *et al.* 2011). The flexible nature of the equatorial region in the

compressed states of ClpP could be explained by the formation of side pores. However, these observations contrast with the findings of a recent study conducted on free and ADEP1-bound *Ec*ClpP using Hydrogen/Deuterium exchange (HDX) coupled with Mass Spectrometry (MS) (Sowole *et al.* 2013). In HDX-MS, deuterium is allowed to exchange with amide backbone H-bonds of a protein, and the resultant time-dependent mass shift is determined by mass spectrometry. Dynamic regions of a protein undergo a rapid deuteration, whereas, the HDX rate is slower in the rigid segments. A noticeabl slow HDX rate observed in the handle domain of ADEP1-bound ClpP suggests the stable nature of the equatorial region. Given the rigid nature of the equatorial region, the authors propose stable equatorial openings for product release.

1.6 Resistance against ADEP1

ADEP1 is produced by *Streptomyces hawaiiensis,* a soil dwelling bacterium. Although *Streptomyces hawaiiensis* is self-resistant against ADEP1, the underlying mechanism of resistance is yet to be elucidated. ClpP exists as a multigene family of five *clpP* genes (*clpP1* through *clpP5*) in most of the sequenced genomes of *Streptomyces.* These genes are arranged as two distinct bicistronic operons, *clpP1clpP2* and *clpP3clpP4,* and a single *clpP5* gene. Interestingly, *S. hawaiiensis* has an additional *clpP* gene known as *clpPAdep,* located among the cluster of genes associated with ADEP1 synthesis. While there is limited knowledge in the literature about the purpose of these operons and homologous ClpP proteins in *Streptomyces,* there is evidence that

clpP1clpP2 are the predominantly expressed genes in wild type. ClpP1 degrades the activator (PopR) of *clpP3clpP4* and controls their expression. However, *clpP3clpP4* are expressed in a *clpP1* deletion strain (Viala, Rapoport and Mazodier 2000, Bellier, Gominet and Mazodier 2006). The monocistronic *clpP5* gene is constitutively expressed under the control of a distinct set of transcription factors compared with other *clpP* operons. Furthermore, ClpP4 and ClpP5 of a number of *Streptomyces* species lack the canonical catalytic triad and are proposed to play a regulatory role similar to their inactive paralogue, ClpR in *Plasmodium falciparum* (Gominet, Seghezzi and Mazodier 2011, El Bakkouri *et al.*).

In vivo studies demonstrate that *S. lividans* is sensitive to ADEP1 (Gominet *et al.* 2011). However, inhibition of ClpP1 results in the expression of ClpP3 and confers ADEP1 resistance in *S. lividans.* In addition to the "target substitution" (ClpP3 substitutes for ClpP1), the study also provides some clues about other still uncharacterized mechanisms for ADEP1 resistance. Given that *S. hawaiiensis* has an additional *clpPAdep* gene in its genome, whether the target substitution or a novel mechanism involving ClpPAdep renders self-resistance against ADEP1 in *S. hawaiiensis* is still to be determined.

Crystal structures of *Ec*ClpP (Li *et al.* 2010) and *Bs*ClpP (Lee *et al.* 2010a) in complex with ADEP1 provided structural insights into the open conformation of the axial gate. The two structures suggested three elements to be essential for a functional axial gate. First, the N-terminal residues of ClpP protomers form an

ADEP1-induced structured β-hairpin. Second, the β-hairpin is stabilized by inter and intramolecular interactions among the N-terminal residues (Li *et al.* 2010). Third, based on the crystal structure of *B. subtilis* ClpP in complex with ADEP1, is the disruption of the hydrophobic cluster region at the base of the β-hairpin (Lee *et al.* 2010a).

In a recent study from our lab, the role of these proposed structural determinants in the open conformation of the axial gate was tested by generating a number of N-terminal variants of *E. coli* ClpP (Alexopoulos *et al.* 2013). In particular, one group of mutants was generated to disrupt the electrostatic interactions amongst the charged residues of the N-terminus. The second group of variants was comprised of amino acid substitutions designed to decrease the likelihood of β-hairpin formation by the N-terminal residues. The third group of ClpP mutants was generated to disrupt the integrity of the hydrophobic cluster region present at the base of the β-hairpin. The effect of changes in the N-terminal region on the ability of ClpP to translocate and hydrolyze substrates of variable sizes was tested using fluorescence based biochemical assays. The study (Alexopoulos *et al.* 2013) concluded that electrostatic interactions among the charged residues of N-terminus of ClpP play a modest role in the open conformation of the axial gate. However, the integrity of the β-hairpin adopted by the N-terminal residues of ClpP protomers and the hydrophobic cluster at its base are the essential requirements for the efficient translocation of substrates through

the axial channel. It was also observed that none of these structural determinants were essential for the translocation of unfolded substrates of small size.

This study identified the structural determinants responsible for a functional axial gate in *E. coli* ClpP. However, it could not address whether the ADEP1 induced gating mechanism is conserved between *E. coli* and *B. subtilis.*

Herein we generated variants of the N-terminal region of ClpP in *B. subtilis* than equivalent to those in *E. coli* and tested their ability to translocate and hydrolyze substrates of variable size using fluorescence based biochemical assays. The mutations showed a similar effect on the translocation of substrates to their counterparts in *E. coli* ClpP. We have also obtained three-dimensional cryo-EM structures of free and ADEP1 bound *E. coli* ClpP. These structures demonstrated an asymmetric nature of the equatorial regions of ClpP with the presence of side pores when ADEP1 is bound. Furthermore, isothermal titration calorimetry (ITC) suggested that 6 molecules of ADEP1 could bind to *Ec*ClpP. These experiments suggested that the conformation and stoichiometry of ADEP1 to *Ec*ClpP in solution is different than observed in the crystal structures.

Finally, we have extended our study to understand the mechanism of ADEP1 resistance in *S. hawaiiensis.* We purified all of the six *Sh*ClpPs. We found that none of the *Sh*ClpPs individually could degrade substrates of variable size or oligomerize as a tetradecamer. None of *Sh*ClpPs could compete with *Ec*ClpP for ADEP1 binding and demonstrated no affinity for ADEP1, as determined by ITC. We also attempted to explore the possibility of a heteromeric ClpP as a functional

protease unit in *S. hawaiiensis.* In this context, we mixed equimolar ratios of *Sh*ClpPs encoded in bicistronic arrangements and examined their oligomeric state. Our extensive investigation could not identify a heteromeric tetradecamer of *Sh*ClpP with the experimental conditions explored in this study. Together, this work has provided further insights into the mechanism of ADEP1 induced activation of ClpP. Though, unable to elucidate the ADEP1 resistance mechanism in *Sh*ClpP, our results constitute the characterization of previously undescribed proteins and provide foundational work for further studies.

2. Material and Methods

2.1 Cloning and purification of wild type and variants of *E. coli* and *B. subtilis* ClpPs

pET9a-ClpP clone to overexpress untagged wild-type *E. coli* ClpP protein was a gift from Dr. Walid Houry (University of Toronto). Wild type *B. subtilis* ClpP gene (GenBank: AAC46381.1) was chemically synthesized (life technologies). Before synthesis, the sequence of *Bs*ClpP gene was optimized using GeneOptimizer software (life technologies) to enhance mRNA stability and translation efficiency in *E. Coli* expression system. The optimized gene was then inserted in pMA-T vector using SfiI cloning sites and the construct was verified by sequencing. The *clpP* gene was then sub cloned in an ampicillin resistant vector expression vector pET21b with NdeI (5′) and XhoI (3′) sites. The final construct included a stop codon to prevent the addition of histidine tag encoded by the vector to the expressed gene.

The *Bs*ClpP mutants were generated using QuikChange Site-Directed Mutagenesis Kit protocol (Stratagene) and sequences were verified by DNA sequencing. Plasmids containing wild type or variants of ClpP were transformed in *E. coli* BL21 (DE3) cells by electroporation using Eppendorf electroporator 2510. Transformed cells were inoculate in Luria Bertani (LB) agar plates containing a final concentration of 30 µg/ml of kanamycin in the case of the plasmid containing *E. coli* ClpP or 100 µg/ml Ampicillin for the *B. subtilis* ClpP plasmid and grown overnight at 37°C. A single colony of cells with successful transformation was inoculated in 50 ml of LB medium containing respective

antibiotics and incubated overnight at 37°C to obtain a primary culture. A volume of 10 ml from the saturated growth culture was sub-cultured in 1 liter culture volumes of LB medium containing appropriate antibiotics and grown at 37°C to an OD_{600} of 0.6. The proteins were overexpressed by adding isopropyl-1-thio-β-D-galactopyranoside (IPTG) up to 1mM and incubating the culture for 4 hours at 37°C. Cells were harvested by centrifugation at 2600 g for 20 minutes using JLA 9.1000 rotor (Beckman).

The cell pellets were washed with 25 ml of PBS buffer (137 mM NaCl, 2.7 mM KCl, 8.1 mM Na_2HPO_4, 1.76 mM KH_2PO_4 at pH 7.4), pelleted again by centrifugation at 4300 g for 20 minutes at 4°C using TS-5.1-500 rotor (Beckman Coulter). At this stage, the cell pellets were flash frozen with liquid nitrogen and stored at -80°C. At the day of purification, the pellets were allowed to thaw in ice and re-suspended in 25 ml of buffer A that contained 50 mM tris-HCl, pH 7.5, 150 mM KCl (50 mM KCl for wild type and variants of *B. subtilis* ClpP), 10% glycerol, and 1 mM DTT. All of the subsequent steps were carried out at 4°C. Protease inhibitors, Benzamidine (156 µg/ml), Phenylmethanesulfonyl fluoride (174 µg/ml), Leupeptin (5 µg/ml) and Pepstatin A (0.7 µg/ml) were added to the cell suspension to inhibit the degradation of ClpP by cellular proteases.

Cells were lysed three times on a pre-chilled French Press at 20000 lb/in^2 and lysates were spun at 30000 g for 40 min at 4°C using Beckman JA 30.5 rotor to precipitate the cellular debris. The supernatants were filtered using 0.45 µm syringe mounted filters (Millex) and loaded onto a HiTrap Q Sepharose HP (GE

Healthcare Life Sciences) anion exchange column equilibrated with buffer A. The column was washed with 5% of buffer B (50 mM tris-HCl, pH 7.5, 1 M KCl, 10% glycerol and 1mM DTT) for 5 column volumes followed by elution of ClpP with 25 % buffer B. 10 µl from each fraction was mixed with sodium dodecyl sulfate (SDS) loading buffer (50 mM Tris-HCl pH=6.8, 2% SDS, 0.1% Bromophenol blue, 10% glycerol, 100 mM β-mercaptoethanol) followed by polyacrylamide gel electrophoresis (PAGE) through a 12 % Bis-Tris gel under denaturing conditions. The gel was stained by Coomassie blue and fractions containing ClpP were pooled, diluted 2X in buffer A (salt free buffer A) and subjected to an 8 ml MonoQ 10/100 column (GE Healthcare). ClpP was eluted with a linear gradient of 5-25% buffer B over 8 column volumes. Fractions were analyzed in a 12% Bis-Tris gel by SDS-PAGE under denaturing conditions.

The fractions containing ClpP were pooled, dialyzed with S200 buffer (50 mM Tris HCl pH 7.5, 200 mM KCl and 10% glycerol) and concentrated to a volume of 500 µl using a 10 kDa cut-off filter (Amicon). The concentrated pool of fractions was further purified by size exclusion chromatography using S200 column 10/30 GL column (GE Healthcare) pre-equilibrated with S200 buffer. Purity of the proteins was verified in a 12% Bis-Tris gel stained by Coomassie blue and fractions containing only ClpP in S200 buffer were pooled and concentrated using a 10 kDa cut-off filter. Concentration of the proteins was determined by taking absorbance at 260 nm using the NanoDrop 2000

Spectrophotometer (Thermo Scientific). The purified proteins were aliquoted, frozen in liquid nitrogen and stored at -80 °C until analysis.

Lopamudra Homchaudhuri; previous post doctorate fellow of Dr. Ortega's lab purified wild type *B. subtilis* ClpP. The N-terminal variant of *E. coli* ClpP in which 9-15 residues were substituted with glycine was purified by John Alexopoulos; former graduate student of Dr. Ortega's lab.

2.2 Isolation of ADEP1

Purified ADEP1 was obtained from Dr. Heike Broetz-Oesterhelt (University of Duesseldorf Institute for Pharmaceutical Biology). The purification was carried out using the fermentation broth of *Streptomyces hawaiiensis* NRRL 15010 according to (Michel and Kastner, 1985) with minor modifications (Li *et al.* 2010).

2.3 Peptide and protein substrates

The substrates of N-Succinyl-Leu-Tyr-7-amido-4-methylcoumarin (Suc-LY-AMC) and fluorescein isothiocyanate alpha casein (FITC α-casein) were purchased from Sigma Aldrich. In Suc-LY-AMC, 7-amido-4-methylcoumarin is the fluorescent compound (excitation=345 nm, emission=440 nm) that is covalently linked to tyrosine. In FITC α-casein, fluorescein isothiocyanate is a chromophore (excitation=490 nm, emission=520 nm), which is bound to α-casein and self-quenches the fluorescence. The substrate of 11-mer peptide (Abz-KASPVSLGYDY^{NO2}) was chemically synthesized by Genscript. In this substrate, 2-aminobenzoic acid (Abz) is the flourophore (excitation=320 nm, emission=440

nm) and 3-nitrotyrosine (Y^{NO2}) is the quencher. An increase in the fluorescence signal indicated the cleavage of these substrates.

2.4 Peptidase and protease activity assays

All of the peptidase and protease activity assays were carried out at 30°C and the reaction components were pre-incubated at 30°C for 5 min before addition of the substrate. Reactions contained 0.14 μM of wild type or variants of $ClpP_{14}$ (*E. coli, B. subtilis, S. hawaiiensis*) and 10 μM of ADEP1. ADEP1 was added from a stock solution with dimethyl sulfoxide (DMSO). Equivalent amount of DMSO was added to the reactions without ADEP1. In the case where the substrate was Suc-LY-AMC dipeptide, a range of 50 μM to 1000 μM of peptide in a total volume of 75 μl was used for steady-state kinetic analysis. Reactions with 11-mer peptide contained a concentration of 1000 μM of peptide in a reaction volume of 75 μl. The buffer used in these two reactions contained 100 mM HEPES (pH 7.25), 10 mM $MgCl_2$, 100 mM KCl, and 10% glycerol. Reactions with FITC α-casein were assembled in a final volume of 50 μl containing 2 mg/ml of the substrate. The reaction buffer used for FITC-α-casein degradation assay was the same as above except it contained 25 mM HEPES (pH 7.25).

In all of the fluorescence-based biochemical reactions the substrate concentration was 3-5 times above the K_m, which was determined to be 214 μM and 753 μg/ml for the 11-mer peptide and FITC-α-casein, respectively. In each case, the fluorescence signal was monitored at the respective wavelengths in a transparent

96-well flat bottom plate (BD Falcon™) using Tecan M1000 Multiplate Reader. The initial rate of the reaction and the graph was plotted as percent initial rate using Microsoft Excel (version 14.3.9, 2011). The K_m and V_{max} and K_{cat} values were calculated by fitting the data into the Michaelis-Menten equation with non-linear regression curve by using GraFit (version 7.0, Erithacus Software. Standard error values were calculated after taking into account the values of each triplicate run.

2.5 Cryo-electron microscopy

For cryo-EM, ClpP samples were diluted in EM buffer (100 mM HEPES pH 7.25, 100 mM KCl, 10 mM $MgCl_2$) to a concentration of 5 µM ($ClpP_1$) and 100 µM of ADEP1 or equivalent amount of DMSO was added to the proteins. 3.4 µl of the reaction mixture was applied onto commercially available c-flat^{TM} holy grids. Prior to deposit the sample, the grids were placed in the Cressington 208 to glow discharge for 15 seconds at 5 mA. Grids were blotted twice for 7 seconds each time and plunged into liquid ethane using a vitrification robot (Vitrobot;FEI). Grids were transferred to a Gatan 914 cryo-holder maintained at liquid nitrogen temperature. Images were recorded on Kodak SO-163 films under low dose settings (~10 e/ Å^2) using the JOEL 2010F, FEG electron microscope operated at 200 KV. A range of 2.5-4.5 µM under-focus was used to collect the images for all data sets. Micrographs were digitalized on Nikon Super COOLSCAN 9000 ED with a step size of 6.35 µm and then binned by the factor of 2 to produce images with a sample size of 2.54 Å /pixel.

2.6 Image processing

A total number of 5000 ClpP particles for 2D and 20,000 particles for 3D analyses were manually picked using Boxer (EMAN). The contrast transfer function parameters of the digitalized micrographs were estimated by using CTFFIND (Mindell and Grigorieff 2003) and subsequently corrected using the Xmipp software package (Scheres *et al.* 2008).

In case of 2D analyses, top view projections of ClpP tetradecamer were selected by cross-correlating the particle images with 2D projections of the reference. The X-ray structure of *E. coli* ClpP (PDB 1TYF) low-pass filtered to 25 Å was used as reference. Particles assigned to the top view projection of the reference map were aligned using reference-free methods to obtain the 2D averages (Scheres *et al.* 2008). After normalization of the 2D averages, the difference maps were calculated using Xmipp software package (Scheres *et al.* 2008). The three-dimensional reconstructions of *Ec*ClpP (with and without ADEP1) were obtained through iterative refinement using 3D projection matching procedures as implemented in the Xmipp 2.4 software package (Penczek, Grassucci and Frank 1994). The reference map used for projection matching approach is same as that used for 2D analyses. To estimate the resolution of the 3D reconstructions, the data was divided into two sets of even and odd numbered particles in the last iteration of refinement. Splitting of the data provided two 3D maps that were used to calculate the Fourier Shell Correlation (FSC) plot. Resolution values (in angstroms) of EM-

maps were obtained from FSC plots using the 0.5 criteria. The cryo-EM maps were visualized in the Chimera program (Pettersen *et al.* 2004).

2.7 Isothermal titration calorimetry (ITC)

All of the ITC experiments were run at 25°C or 37°C. An unmatched buffer of the reactants and presence of glycerol or DMSO has an enormous effect on ITC signal. Our reactants were stored in buffers that were unacceptable for ITC analyses since ADEP1 is dissolved in 100% DMSO and the storage buffer of ClpPs contains 10% glycerol. Therefore, it was important to remove or reduce the amounts of glycerol and DMSO and match the buffers of working solutions of ADEP1 and ClpPs. This was achieved by diluting ADEP1 stock in ITC buffer (50 mM TrisHCl, pH 7.5, and 200 mM KCl) to a concentration of 300 µM, which gave a final concentration of 1% DMSO (acceptable for ITC). Matching of ClpP buffers to that of ADEP1 and removal of glycerol was accomplished by dialyzing the proteins in ITC buffer that contained 1% DMSO. Dialysis of proteins was achieved using 500 µL Nanosep Centrifugal Devices (Pall Corporation) with molecular weight cut-off value of 10 KDa. Prior to use, the devices were washed twice with ITC buffer to remove residual glycerol and sodium azide.

Once ADEP1 and ClpPs were in matching buffers, 300 µL of 50 µM ClpP (monomer) was loaded into the sample cell of a Nano Isothermal Titration Calorimeter 601002 (TA Instruments) and stirred constantly at 250 rpm. The Nano syringe was filled with 50 µL of 300 µM ADEP1 solution (previously degassed at 20°C). ADEP1 was titrated into the sample cell in 2 µl injections at

120 seconds intervals. Titration of buffer (-ADEP1) into buffer (-ClpP) provided the background heats of dilution, which were subtracted from the experimental data to obtain the net binding. Least squares regression to identical independent binding sites model was used to calculate the number of binding sites and kd using NanoAnalyze software (TA instruments). Running 1000 trials for the Gaussian distribution of standard deviation around the fit with 95 % confidence interval validated the quality of fitting raw data into the model.

2.8 Cloning and purification of *Sh*ClpPs

Plasmids (pET28a) containing *S. hawaiiensis clpP* genes (*clpP1*, *clpP2, clpP3, clpP4, clpP5* and *clpPAdep*) with N-terminal histidine tag were a generous gift from Dr. Eric Cheng (University of Wisconsin). The genes had been incorporated into the vector using NdeI and HindIII sites. To generate the clones capable of expressing the ClpP proteins without an N-terminal histidine tag, the NcoI site upstream of the histidine tag sequence was mutated to an NdeI site using QuikChange site-directed mutagenesis method (Stratagene) (work performed by John Alexopoulos; former MSc student in the Ortega lab). Subsequently the plasmids were digested with NdeI (Thermo Scientific), followed by gel extraction using Qiaex II kit (Qiagen), and re-ligation using T4 DNA ligase (Novagen) to generate the clones without any histidine tag to express proteins of native sequence.

pET28a-*Sh*ClpP1 was transformed into *E. coli* BL21 (DE3) and the clones of pET28a-*Sh*ClpP2, pET28a-*Sh*ClpP3, pET28a-*Sh*ClpP4, pET28a-*Sh*ClpP5, pET28a-*Sh*ClpPAdep were transformed into *E. coli* BL21 Star (DE3) pRARE2 competent cells (Novagen) by electroporation. The expression and purification of *Sh*ClpPs were

performed following a similar protocol to that used for *E. coli* and *B. subtilis* ClpP with some modifications. Briefly, cells were grown in 1L of LB medium at various temperatures using either kanamycin or with chloramphenicol (Table1) to an OD_{600} of 0.6. Expression of *Sh*ClpPs was induced with various concentrations of IPTG ranging from 0.01 mM to 1 mM. Following induction, the cells were grown at either 25°C or 37°C ranging from 4 to 16 hours (Table1).

Table 1: Conditions for the expression and purification of the *Sh*ClpPs.

	***Sh*ClpP1**	***Sh*ClpP2**	***Sh*ClpP3**	***Sh*ClpP4**	***Sh*ClpP5**	***Sh*ClpPAdep**
Antibiotic	Kanamycin	Kanamycin + chloramphenicol	Kanamycin + chloramphenicol	Kanamycin + chloramphenicol	Kanamycin + chloramphenicol	Kanamycin + chloramphenicol
IPTG	1 mM	1 mM	1 mM	0.5 mM	0.01 mM	0.01 mM
Time and temperature during induction	16 hours at 37ºC	5 hours at 25ºC	5 hours at 25ºC	5 hours at 25ºC	8 hours at 25ºC	4 hours at 37ºC
Ammonium sulfate precipitation	30-50%	30-60%	NA	30-50%	30-50%	30-60%
Gradient of Buffer B	5-35%	5-16%	5-16%	5-25%	5-16%	5-20%

Cells were harvested and lyzed as described in section 2.1. Cellular debris was cleared using centrifugation at 30000 g for 40 min at 4°C using Beckman JA 30.5 rotor and the supernatant was collected. The supernatant (25-30 ml) was diluted to a final volume of 80 ml with buffer A (50 mM tris-HCl, pH 7.5, 50 mM KCl).

For all *Sh*ClpPs except for *Sh*ClpP3, ammonium sulfate was slowly added to the cleared supernatant for over 2 hours while magnetic stirring at 4ºC to a final concentration of 30%. The supernatant was allowed to stir slowly for another

hour followed by centrifugation at 4300 g for 20 min using TS-5.1-500 rotor (Beckman Coulter) to clear the precipitated proteins. The supernatant was recovered and the concentration of ammonium sulfate was brought up to 50% (60% for *Sh*ClpPAdep) under the same conditions. The precipitated protein was pelleted by centrifugation at 4300 g for 20 min at 4ºC using TS-5.1-500 rotor (Beckman Coulter). The pellet was re-suspended in 10 ml of buffer A and dialyzed overnight at 4ºC into buffer A. The dialyzed proteins (supernatant of the cell lysate in case of *Sh*ClpP3) was filtered through 0.45 µm syringe mounted filters (Millex) and loaded onto a HiTrap Q Sepharose HP (GE Healthcare Life Sciences) anion exchange column equilibrated with buffer A. The column was washed with 5% of buffer B (50 mM tris-HCl, pH 7.5, 1 M KCl, 10% glycerol and 1mM DTT) for 5 column volumes. The proteins were eluted with a linear gradient from 5-35% of buffer B over 15 column volumes (Table1). Fractions were analyzed in a 12% Bis-Tris gel by SDS-PAGE and fractions containing *Sh*ClpP were diluted into buffer A (salt free buffer A) to bring the salt concentration to 50 mM KCl.

The pooled fractions were subjected to a second anion exchange MonoQ 10/100 column (GE Healthcare Life Sciences) pre-equilibrated with buffer A. *Sh*ClpPs were eluted with a linear gradient of 5-35% buffer B over 10 column volumes as used during HiTrap Q Sepharose HP column purification. From this step onward the purification of all six *Sh*ClpPs was identical. Fractions were analyzed in a 12% Bis-Tris gel by SDS-PAGE and those containing *Sh*ClpP were

pooled, dialyzed with S200 buffer (50 mM Tris HCl pH 7.5, 200 mM KCl and 10% glycerol) and concentrated to a volume of 500 µl using a 10 kDa cut-off filter (Amicon). This concentrated pool of fractions was further purified using size exclusion chromatography using S200 column 10/30 GL column (GE Healthcare) pre-equilibrated with S200 buffer. *S. hawaiiensis* ClpPs eluted at approximately 15-16 ml corresponding to monomers of ~21-25 kDa. Purity of the proteins was verified in a 12% Bis-Tris gel stained by Coomassie blue and fractions containing purely ClpP in S200 buffer were pooled and concentrated using a 10 kDa cut-off filter. Concentration of the proteins was determined by taking absorbance at 260 nm using the NanoDrop 2000 Spectrophotometer (Thermo Scientific). The proteins were aliquoted, frozen in liquid nitrogen and stored at -80 °C until analysis.

Harsh Desai and Lydia Xing carried out purification of *Sh*ClpP2 and *Sh*ClpP4, respectively. Both are former undergraduate students of Dr. Ortega's lab.

2.9 Competition assay

Competition assay was performed as described in (Alexopoulos *et al.* 2013). In the control reaction, degradation of FITC α-casein by ADEP1-activated wild type *E. coli* ClpP is monitored after adding increasing amount of catalytically inactive ClpP ($ClpP_{in}$) into the reaction. $ClpP_{in}$ cannot degrade FITC α-casein but can sequester ADEP1 from the active wild type *E. coli* CpP, which decreases the initial rate of the reaction. Conversely, if *Sh*ClpPs are unable to compete for

ADEP1 will not affect the rate of the reaction when additional amount of the protein is included. Since *E. coli* ClpP degrades FITC α-casein and none of the *Sh*ClpPs could hydrolyze it, therefore the fluorescence signal can only be attributed to degradation of the substrate by ADEP1-activated wild type *E. coli* ClpP.

Wild type *E. coli* ClpP was proteolitically inactivated ($ClpP_{in}$) by treating with carbobenzoxy-Leu-Tyr-chloromethylketone (Bachem) as previously described (Singh, Guo and Maurizi 1999). Briefly, a stock (20 mg/mL) of the inactivator dissolved in DMSO was used to prepare a reaction mixture containing five-fold molar excess of the inactivator over *E. coli* ClpP. The reaction was incubated at room temperature for 40 min with gentle agitation. The reaction tube was then spun down at 13,000 g at 4 ^{o}C for 10 min in a bench top microcentrifuge (Eppendorf). Approximately 300 µL of supernatant was diluted with 5 mL of buffer containing 50 mM Tris HCl pH 7.5, 200 mM KCl, 10% glycerol, and the mixture concentrated with a 10 kDa cut-off filter to remove the carbobenzoxy-Leu-Tyr- chlorome-thylketone reagent. This step was repeated for two more times. Pre and post treated ClpP was tested for its peptidase activity, where post treated ($ClpP_{in}$) appeared catalytically inactive. *Sh*ClpPs do not have activity against FITC α-casein thus it was not necessary to chemically inactivate *Sh*ClpPs. The competition assay was performed as the FITC α-casein assay. The concentrations of a chemically inactivated variant of ClpP ($ClpP_{in}$) or one of the

*Sh*ClpPs were increased stepwise but in independent reactions. Standard error values were calculated after taking into account the values of each triplicate run.

2.10 Size exclusion chromatography to determine the oligomeric state of ShClpPs

A total amount of 30 µg of ClpP dissolved in 10 µl of S200 buffer (Tris-HCl pH 7.5, 200 mM KCl, 50 mM 10% glycerol) was loaded onto a Superdex 200 PC 3.2/30 (GE Healthcare) pre-equilibrated with S200 buffer. Five-fold molar excess of ADEP1 to that of ClpP monomer was mixed with the protein and incubated at room temperature for 15 min, 5 hours and overnight in the cases when size exclusion chromatography was performed in the presence of ADEP1. Reading absorbance at 230 nm followed elution profiles of the proteins.

2.11 Electron Microscopy

To visualize the oligomeric state of *Sh*ClpPs, the proteins were imaged using negative stain electron microscopy as described earlier (Ortega *et al.* 2000). The fractions from size exclusion chromatography representing the peaks were collected and diluted to a concentration of 30 µg/ml in S200 buffer. 5 µl of the diluted sample was floated onto freshly prepared carbon coated grids after glow discharge. After 2 minutes, the grids were blotted and stained with 1% uranyl acetate for 1 minute. Specimens were imaged on a JEOL 1200EX electron microscope operated at 80 kV using a nominal magnification of 300000X.

2.12 Protein sequence alignment

Sequence alignments of ClpPs from *S. hawaiiensis* (NRRL 15010) and *S. lividans* (1326) were created using online alignment software tool clustalW (http://www.ebi.ac.uk/Tools/msa/clustalW2/).

3. Results

3.1 Electrostatic interactions play a modest role in mediating the open conformation of the axial gate of ClpP in *Bacillus subtilis*

The crystal structure of *Ec*ClpP in complex with ADEP1 (Li *et al.* 2010) shows that N-terminal residues of each ClpP protomer adopt a β-hairpin upon ADEP1 binding. Two types of electrostatic interactions stabilize this conformation of N-terminal residues. First, in each protomer, the intramolecular interaction between Glu8 with the side chains of Lys25 in the globular domain of ClpP retracts the β-hairpin from the axial lumen. Second, the intermolecular interactions between Glu14 and Arg15' (indicates residue of neighbouring protomer) fasten the N-terminal loops forming a rigid rim for the axial pore.

We generated two variants of *Bs*ClpP to test the importance of these intra- (Glu8-Lys25) and intermolecular (Glu14-Arg15') interactions in stabilizing the open conformation of the axial pore in *B. subtilis* ClpP. We substituted the residues involved in these interactions with alanine. In one of the variants, the wild type N-terminal sequence of *B. subtilis* ClpP ^{8}EQTNRGER^{15}+K^{25} was transformed into ^{8}EQTNRG<u>AA</u>^{15}+ K^{25} (substituted residues are underlined) to eliminate the intermolecular interactions between Glu14 and Arg15'. Additionally, the wild type sequence ^{8}EQTNRGER^{15}+K^{25} was mutated to ^{8}EQTNRG<u>AA</u>^{15}+<u>A</u>^{25} to generate a variant that abolished both inter or intramolecular interactions. Afterwards, in a fluorescence-based assay we measured the hydrolysis rates of the variants for fluorescein isothiocyanate alpha casein (FITC α-casein), in which casein is the substrate for ClpP. The ClpP variant ^{8}EQTNRG<u>AA</u>^{15}+ K ^{25} with

disrupted intermolecular interactions had a hydrolysis rate that was slightly higher than wild type. The second variant ^{8}EQTNRGAA^{15}+A^{25} that could not establish either inter or intramolecular interactions showed moderately reduced proteolytic activity against FITC α-casein (Figure 5A). These results indicate that the intermolecular interactions between Glu14 and Arg15' are not essential in stabilizing the open conformation of the axial gate. However, in combination, the intra (Glu8-Lys25) and intermolecular (Glu14 and Arg15) interactions moderately contribute towards the maintenance of the open conformation of the axial gate. These results are in agreement with the findings for equivalent variants of *E. coli* ClpP (Alexopoulos *et al.* 2013).

3.2 Structured β-hairpin is essential for the open conformation of the axial gate

The X-ray structure of *Ec*ClpP in complex with ADEP1 (Li *et al.* 2010) shows that N-terminal residues of each ClpP protomer adopt a structured β-hairpin upon ADEP1 binding. Conversely, these residues are not visible in the X-ray structure of *B. subtilis* ClpP in complex with ADEP1 and are proposed to become flexible upon ADEP1 binding (Lee *et al.* 2010a). We needed to test whether formation of a β-hairpin by the N-terminal region was required for the axial pore of *B. subtilis* ClpP to efficiently translocate protein substrates. In this context, we constructed three N-terminal variants of *B. subtilis* ClpP, aiming to decrease the likelihood of β-hairpin formation. First, by substituting Glu14 and Arg15' with glycine residues, we mutated the wild type N-terminal sequence ^{8}EQTNRGER^{15}+K^{25} to ^{8}EQTNRGGG^{15}+K^{25}. Glycine is known to destabilize the

secondary structure elements (Chou and Fasman 1974). A secondary structure predication of the ^{8}EQTNRGGG^{15}+K^{25} variant is that there would be a lower likelihood for the N-terminus to adopt a β-hairpin conformation (Alexopoulos *et al.* 2013 Fig 3A). This variant retained 64% of the proteolytic activity compared to wild type when tested against FITC α-casein (Figure 5A). This result indicates that minimal disruptive change in the secondary structure of N-terminal residues aimed to decrease the likelihood of β-hairpin conformation moderately affected the translocation of FITC α-casein.

The second variant was designed to drastically reduce the ability of the N-terminus to adopt a β-hairpin conformation. In this case, we mutated the wild type N-terminal sequence of *Bs*ClpP ^{8}EQTNRGER^{15}+K^{25} to ^{8}EGGGGGGG^{15}+K^{25}. Secondary-structure prediction for the N-terminus of *Ec*ClpP with these mutations suggests a markedly reduced likelihood of N-terminal residues to adopt a β-hairpin conformation (Alexopoulos *et al.* 2013 Fig 3A). A third variant aiming to introduce a kink in the chain of the N-terminus to decrease the likelihood of β-hairpin formation was generated by substituting isoleucine 7 with proline. We noticed that in the X-ray structure of *Ec*ClpP (Li *et al.* 2010) a kink in the main chain of the N-terminus of ClpP caused by Pro4 is important for defining the conformation of the loop. The rationale for constructing the I7P variant was to introduce another kink in the main chain of the N-terminus of ClpP and disrupt its conformation. A secondary structure prediction showed that the I7P mutation causes the N-terminus of *Ec*ClpP to adopt a coil conformation (Alexopoulos *et al.*

2013 Fig 3A). When hydrolysis was tested using FITC α-casein, we observed that the hydrolysis rate of the substrate decreased to 10 % and 20 % for the ^{8}EGGGGGGG^{15}+K^{25} and I7P mutants respectively (Figure 5A).

Together, these results indicate that relatively less disruptive changes (^{8}EQTNRGGG^{15}+K^{25}) in the secondary structure of N-terminal residues moderately affected the translocation of FITC α-casein. When more drastic changes were introduced into ClpP (^{8}EGGGGGGG^{15}+K^{25} and I7P) the ability to translocate substrates into the axial channel was severely compromised. Therefore, we conclude that formation of a structured β-hairpin by the N-terminal residues of ClpP is an essential requirement for the efficient translocation of substrate. These observations are consistent with the observed findings in the equivalent variants of *E. coli* ClpP (Alexopoulos *et al.* 2013).

ClpP can hydrolyze peptides of 10 amino acids in the presence of ATPases or ADEP1 (Lee *et al.* 2010a, Lee *et al.* 2010b, Li *et al.* 2010). To test the ability of *B. subtilis* ClpP variants to degrade unfolded substrate of relatively small size, an 11-mer peptide labeled with the fluorophore 2-aminobenzoic acid (ABZ) and the quencher 3-nitrotyrosine (Y^{NO2}) was used as the substrate. In the absence of ADEP1, *B. subtilis* ClpP (wild type and mutants) could not degrade this substrate due to their inability to oligomerize. However, addition of ADEP1 resulted in substrate hydrolysis and all of the *B. subtilis* ClpP variants showed a hydrolysis rate that was equal or comparable to wild type (Figure 5B).

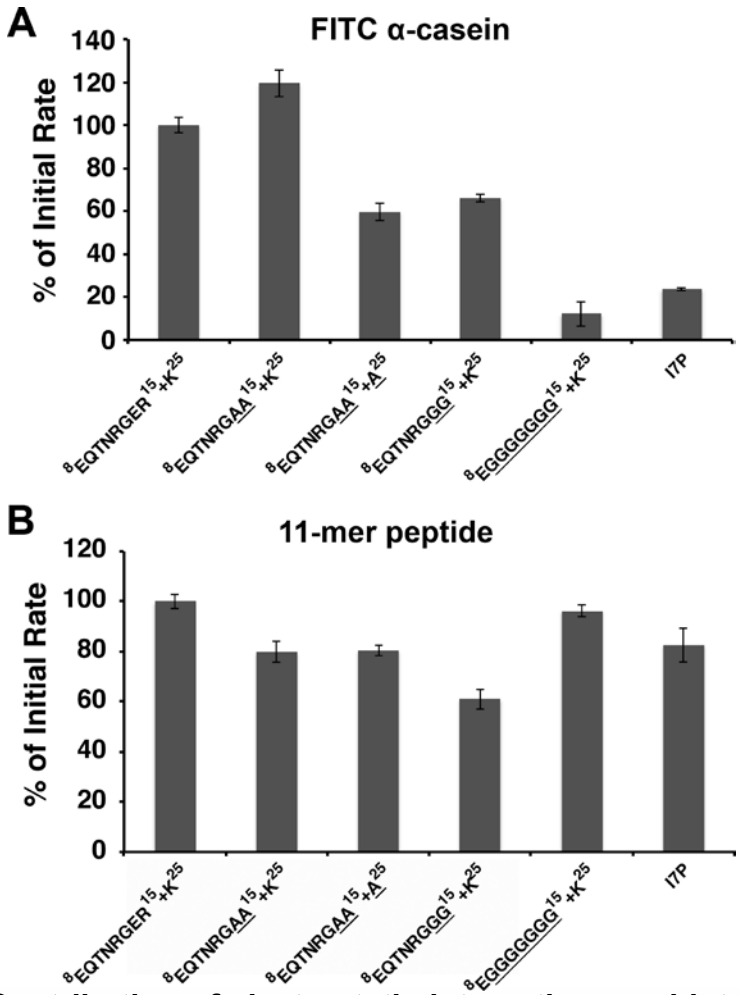

Figure 5: Contribution of electrostatic interactions and integrity of β-hairpin to the stability of the open conformation of the axial gate and subsequent substrate translocation. The wild type *Bs*ClpP is indicated by ^{8}EQTSRGER^{15}+K^{25} whereas the variants are named according to the N-terminal amino acid sequence 8 through15 and 25. The underlined residues indicate the substituted amino acids. The initial rate of FITC α-casein **(A)** and 11-mer peptide hydrolysis **(B)** obtained with wild-type ClpP was defined as 100% and initial rates for all variants were plotted relative to this. All reactions were carried out in the presence of 10 μM of ADEP1. The errors bars represent standard deviation obtained from at least three experimental replicas of each reaction.

These findings suggested that compromising the electrostatic interactions or disrupting β-hairpin formation did not prevent entry of the 11-mer peptide into the degradation chamber of ClpP. A maximum reduction in hydrolysis rate was observed in the ^{8}EQTNRGGG^{15}+K^{25} variant that still retained 62% of the wild type activity (ref. discussion). Equivalent variants of *E. coli* ClpP displayed a hydrolysis rate that was comparable to or even higher than the wild type (Alexopoulos *et al.* 2013). These results suggest that the previously identified structural determinants that stabilize the open conformation of the axial gate are not essential to preclude the entry of unfolded substrates of smaller size into the catalytic chamber of ClpP.

3.3 Two-dimensional cryo-EM structures validate the secondary structure predictions

The results obtained from the study of *E. coli* (Alexopoulos *et al.* 2013) and *B. subtilis* ClpP (herein) suggest that the mechanism of ADEP1-induced activation of ClpP is conserved in both organisms. Based on biochemical data, these studies identified the structural determinants responsible for a functional axial gate but lacked the experimental validation of secondary structure predictions considered while designing the N-terminal variants of ClpP. To this end, we used cryo-EM for structural analysis of *B. subtilis* ClpP (wild type/variants) in the presence or absence of ADEP1. Given that *B. subtilis* ClpP requires ADEP1 for oligomerization, it was not possible to obtain cryo-EM structures of ADEP1-free *Bs*ClpPs. Therefore, an accurate validation of predicted changes in the secondary structure of the N-terminus of ClpP could not be made.

Conversely, *E. coli* ClpP is not dependent on ADEP1 for oligomerization. Hence, we structurally analyzed wild type *E. coli* ClpP and its variant ^{8}EGGGGGGG^{15}+K^{25} in the presence and absence of ADEP1. The presence of multiple glycine residues offers a high degree of flexibility and a drastic change in the secondary structure making this variant the most suitable candidate for structural work. Cryo-EM data was subjected to image processing and top view projections were selected and aligned to calculate a 2D projection for each sample.

Overall, 2D averages of all four samples appeared to have similar structural features, for instance, seven globular densities, each representing a ClpP protomer. However, a noticeable difference was observed in the amount of density present in the axial channel. This density was diffuse in the case of wild type ClpP (-ADEP1), consistent with the N-termini of free ClpP occluding the axial channel to block the substrate access to the catalytic chamber (Figure 6).

Conversely, a well-defined axial pore of ~18Å without appreciable density in the axial channel was observed in the 2D average of wild type ClpP (+ADEP1). By subtracting the 2D average of *Ec*ClpP (+ADEP1) from *Ec*ClpP (-ADEP1), a difference map was obtained to better visualize the differences in the axial pore. The calculated difference map verified that the amount of density in 2D average of *Ec*ClpP (-ADEP1) is greater than the density present in the axial channel of the 2D average of *Ec*ClpP (+ADEP1) (Figure 6). It could be inferred that either the N-termini had been retracted from the axial lumen, as suggested by the crystal

structure of *E. coli* ClpP in complex with ADEP1 (Li *et al.* 2010) or became flexible and thus not visible, as proposed by the crystal structure of *B. Subtilis* in complex with ADEP1 (Lee *et al.* 2010a).

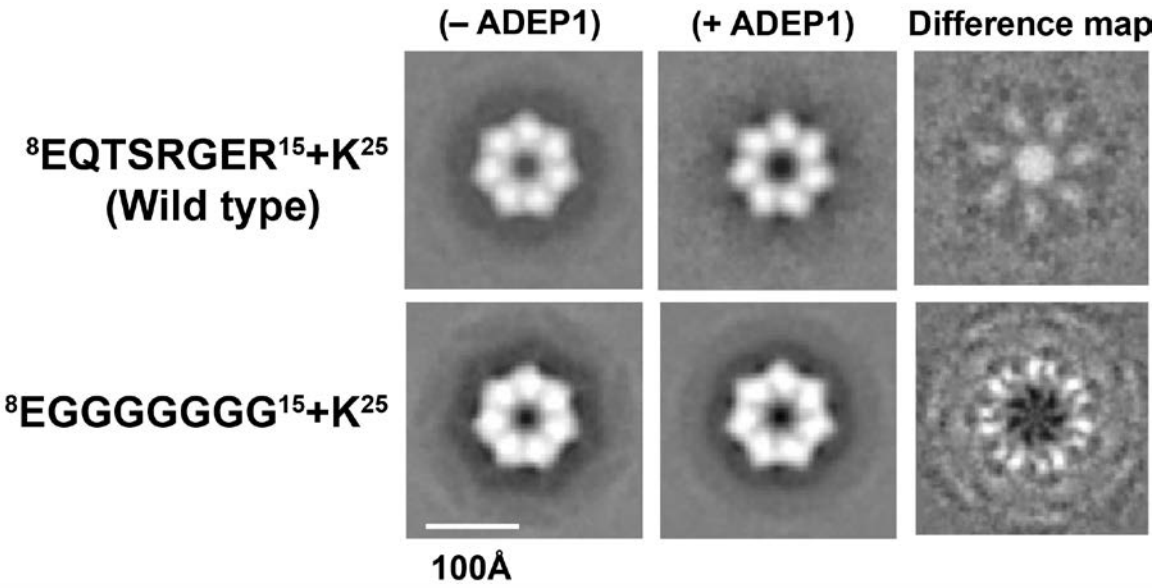

Figure 6: Validation of secondary structure predictions by 2D structural analyses. 2D averages obtained from the top view projections of wild type *Ec*ClpP and its variant in which residues 9-15 were substituted with glycine. The difference maps were calculated by subtracting the 2D average of ClpP obtained in the presence of ADEP1 from that obtained in the absence of the antibiotic. The contrast of 2D averages was normalized before calculating the difference maps.

Cryo-EM images of ^{8}EGGGGGGG^{15}+K^{25} (ADEP1) were processed in an identical way as the wild type *E. coli* ClpP samples. A diffuse amount of axial density was observed in the 2D averages of this variant in the presence and absence of ADEP1. However, the calculated difference map displayed greater amount of axial density in the 2D average obtained from the sample that was imaged in the presence of ADEP1 (Figure 6). This result corroborated that N-termini of ^{8}EGGGGGGG^{15}+K^{25} variant blocked the axial channel of ClpP upon

ADEP1 binding. These results validate the secondary structure predictions that were considered while designing the N-terminal variants of ClpP.

3.4 Role of the hydrophobic cluster at the base of the N-terminal β-hairpin for a function axial gate of ClpP could not be tested in *B. subtilis*

A third element we observed in the X-ray structure of *E. coli* ClpP (Li *et al.* 2010) important for stabilizing the secondary structure adopted by the N-terminal region is a hydrophobic cluster of residues at the base of the hairpin. Residues integrating this cluster include Val6 and Ile19 of one protomer and Leu24 and Phe49 of the adjacent protomer. To test the importance of this structural element in the gating mechanism of ClpP, an I19A variant was generated in *Ec*ClpP and its hydrolysis rate of FITC α-casein was measured. A substantial reduction (90%) in hydrolysis rate suggested that the integrity of the hydrophobic cluster region is also an important requirement for a functional axial gate in *Ec*ClpP (Alexopoulos *et al.* 2013 Fig 3A). It was not possible to test this variant of *B. subtilis* ClpP as the I19A substitution prevents the oligomerization of ClpP to a tetradecamer (Lee *et al.* 2010a).

3.5 Mutations in the N-terminal region did not affect the catalytic activity of *Bs*ClpP

Fluorescence based biochemical assays performed in this study measured the hydrolysis rates of ClpP variants against FITC α-casein and an 11-mer peptide. The data obtained in these assays is reflective of combined efficiency of translocation and hydrolysis of FITC α-casein or 11-mer peptide by wild type or a particular variant of ClpP. Therefore, it was important to establish whether the

difference in the hydrolysis rates was exclusively due to the change in the ability of *Bs*ClpP variants to translocate protein substrates. To this end, we used a fluorogenic dipeptide; N-Succinyl-Leu-Tyr-7-amido-4-methylcoumarin (SLY-AMC) as a substrate. This dipeptide can diffuse freely into the catalytic chamber of ClpP and its hydrolysis rate is independent of translocation ability of ClpP. All of the *Bs*ClpP variants retained their ability to hydrolyze dipeptides (Table 2).

Table 2. Kinetic parameters of *B. subtilis* N-terminal ClpP variants with Suc-LY AMC peptide.

***Bacillus subtilis* ClpP 2mM + 10 µM ADEP1**	**K_m (µM)**	**k_{cat} (RFU x s^{-1} μM^{-1})**
^{8}EQTNRGER^{15}+K^{25} (Wild Type)	315 ± 55	4.2 ± 0.6
^{8}EQTNRGAA^{15}+K^{25}	270 ± 110	2.8 ± 0.4
^{8}EQTNRGAA^{15}+A^{25}	130 ± 40	2.1 ± 0.2
^{8}EQTNRGGG^{15}+K^{25}	280 ± 40	3.8 ± 0.2
^{8}EGGGGGGG^{15}+K^{25}	110 ± 30	1.5 ± 0.1
I7P	300 ± 50	1.6 ± 0.1

RFU: Relative Fluorescence Units.

These results implicate that the mutations in the N-terminal region of *Bs*ClpP did not abolish the ability of the enzyme to hydrolyze peptide bonds and the difference in the hydrolysis rates of substrates by the *Bs*ClpP variants were due to the variations in their ability to translocate substrates. These results are

comparable to the wild type and equivalent variants generated in *Ec*ClpP (Alexopoulos *et al.* 2013).

3.6 ADEP1-bound *Ec*ClpP adopts a different conformation in solution than observed in the X-ray structure

The discrepancies between the X-ray structures of ClpP in complex with ADEP1 (Li *et al.* 2010, Lee *et al.* 2010a) raise the question whether the conformation of ClpP in the crystal structures is descriptive of its conformation in solution. In this context we used cryo-EM to obtain the 3D structure of *Ec*ClpP in solution both in the presence and absence of ADEP1. The 3D cryo-EM structure of *Ec*ClpP (-ADEP1) lacked top to bottom symmetry and the structural features on the axial surfaces were different. Both axial pores appeared to be blocked by densities, however, the longitudinal cross-section showed a relatively large density on the end assigned as 'bottom'. The second end, assigned as 'top', displayed a density that progressively reduced while radiating from the periphery to the central axis (Figure 7 left panel).

Interestingly, the 'top' end of the ClpP structure underwent a conformational change, blocking the axial channel when ADEP1 was added to the sample. Conversely, a ADEP1-induced conformational change in the 'bottom' end generated a pore of ~18 Å that was initially blocked by a large amount of density (Figure 7 right panel). The secondary structural elements of the N-terminal region could not be resolved in the EM-map at the resolution of ~16Å. However the size of the axial pore is comparable to that observed in the crystal structure of *Ec*ClpP in complex with ADEP1.

In addition to the conformational changes on the axial sites, we observed side pores measuring ~10Å in length in one of the ClpP heptamers (Figure 7). A minimal hydrogen deuterium exchange rate (HDX rate) in the handle region of the ClpP monomer (Sowole *et al.* 2013) suggests that the handle domain is stabilized upon ADEP1 binding. The presence of well-defined side pores in our cryo-EM structure, and minimal HDX rate in the handle region of the ClpP monomer (Sowole *et al.* 2013) complement each other and suggests that these pores are stable in nature. Existence of side pores in the equatorial region of ClpP has been reported by several biochemical and structural studies in *S. aureus*, *B. subtilis,* and *E. coli* (Kimber *et al.* 2010, Lee *et al.* 2011, Sprangers *et al.* 2005, Ye *et al.* 2013). Our results are in agreement with the published data about the stable presence of side pores, but differ regarding their location.

In our 3D-EM structure of ClpP in complex with ADEP1, side pores are visible slightly off the equatorial part of the tetradecamer and only in one of the heptamers. In the X ray structures (Kimber *et al.* 2010, Lee *et al.* 2011) these side pores are located on the equatorial region. The asymmetric nature of the two heptamers observed in the 3D-EM structure of ClpP in complex with ADEP1 suggests that *Ec*ClpP adopts a different conformation in solution than observed in the X-ray structures.

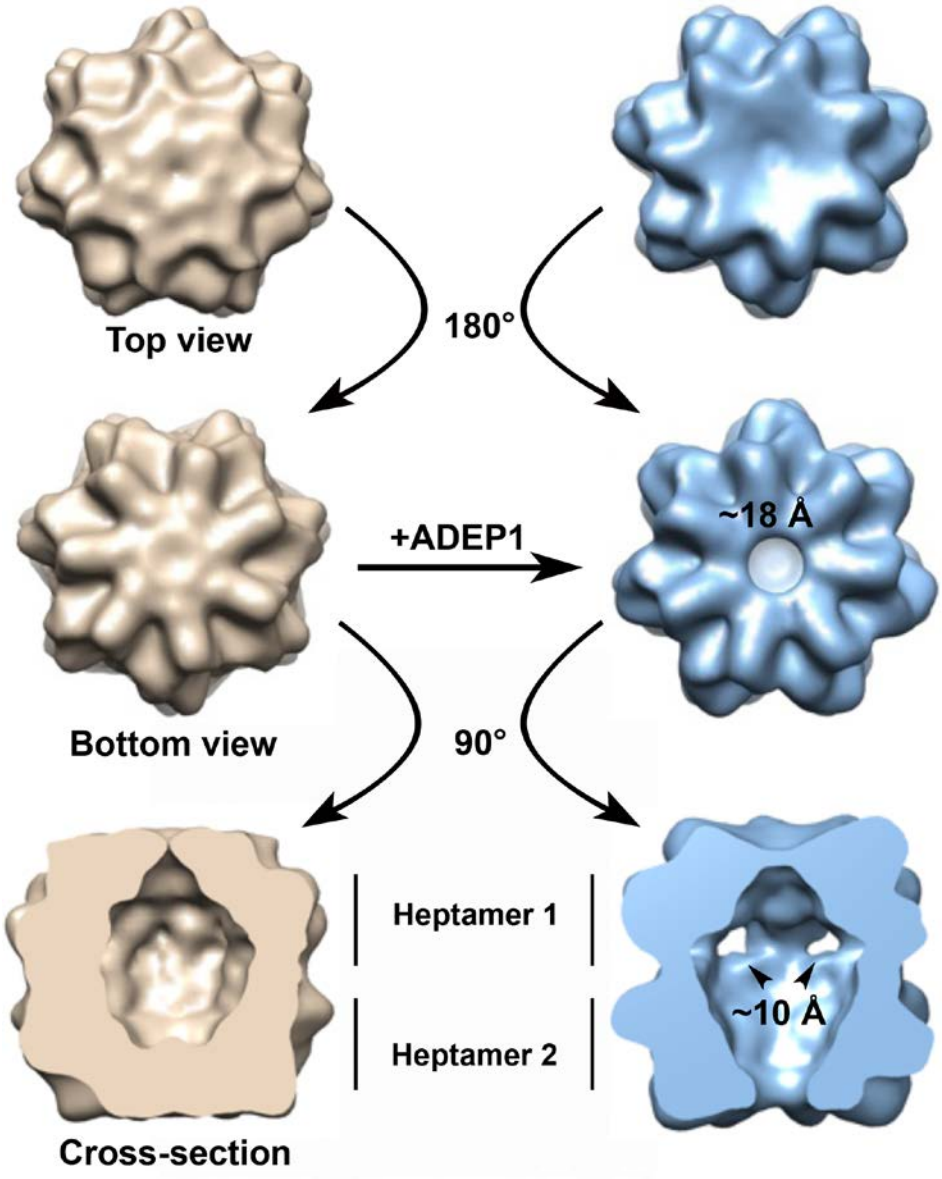

Figure 7: Three-dimensional cryo-EM maps of *E. coli* ClpP. Projections of cryo-EM structures of wild type *E. coli* ClpP in the absence (left panel) and presence of ADEP1 (right panel). EM-maps have been colored differently and one of the ends is assigned as 'top view' while the other as 'bottom view' of ClpP for differentiation. The cross-section demonstrates the thickness of density of the ClpP maps at the both ends. The resolution of EM-maps is 13Å and 16Å for *E. coli* ClpP in the absence and presence of ADEP1, respectively. The resolution was estimated using a Fourier Shell Correlation (FSC) 0.5 criterion without low-pass filtering the reference in the last iteration of projection matching. Arrowheads highlight the presence of side pores of ~10Å in length in heptamer 1.

3.7 *Ec*ClpP in solution binds to six molecules of ADEP1

Whether *Ec*ClpP binds to 14 molecules of ADEP1 in solution could not be established by cryo-EM. In this context, we used Isothermal Titration Calorimetry to measure how many molecules of ADEP1 were bound to a ClpP tetradecamer. ITC works on the principle of measuring heat release when a ligand binds to the macromolecules, until maximal occupancy of the ligand has been reached for the enzyme. Since the experiments were performed in solution, it was possible to measure stoichiometry and affinity of ClpP for ADEP1 under the conditions that mimicked the cryo-EM.

The ITC data were analyzed by allowing the number of binding sites (n) to vary and subtracting the blank from the experimental data. The data fit well to the least squares regression to independent binding sites model and calculated six (5.95 ± 0.35) molecules of ADEP1 bound to an *Ec*ClpP tetradecamer (Figure 8A). The X-ray structure of *Ec*ClpP (Li *et al.* 2010) shows fourteen (7 per heptameric ring) hydrophobic pockets occupied by the same number of ADEP1 molecules. In order to determine whether the ITC data was consistent with the binding of 14 molecules of ADEP1 to the tetradecamer, we fixed the number of binding sites to 14 and fit the data using the same model. The data could not fit into the model suggesting that binding of 14 molecules of ADEP1 to ClpP is not consistent with the ITC data (Figure 8).

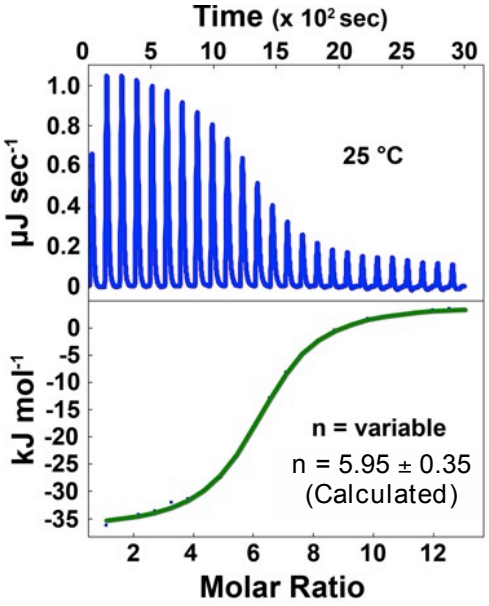

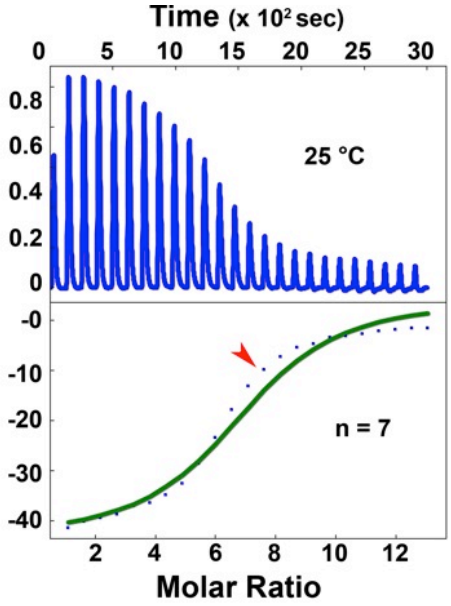

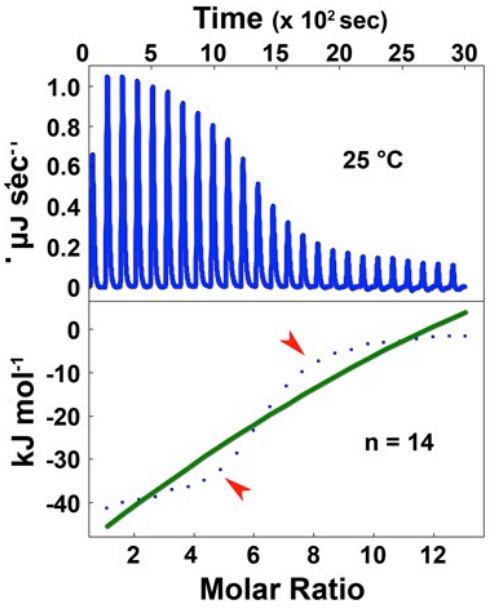

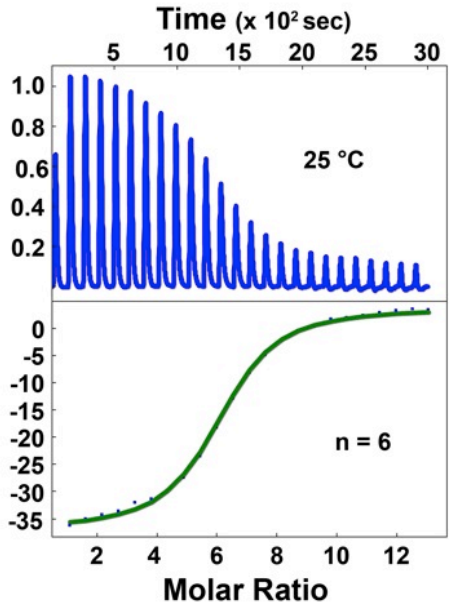

Parameters	n = variable	n = 6	n = 7	n = 14
K_d µM	0.33 (0.04)	0.33 (0.01)	1.069 (0.01)	78.34 (1.56)
ΔH kJ/mol	-34.87 (4.2)	-34.48 (0.6)	-39.26 (0.70)	-259.6 (5.7)
ΔS J/mol-K	8.091 (0.8)	8.286 (0.16)	-17.35 (0.31)	-792.2 (17.4)
ΔG kJ/mol	-37.25 (0.1)	-59.17 (1.1)	1.24 (0.02)	233.48 (5.1)

Figure 8: Binding of ADEP1 to *Ec*ClpP as determined by ITC. ITC data for heat released (blue peaks) due to binding of ADEP1 to *Ec*ClpP (Top left panel). Each peak indicates heat released after an injection of ADEP1 during titration until the saturation point was reached. The resultant binding sigmoidal curve in green color represents fitting of the data into an identical binding site model. The heat released as a result of first reaction was excluded while modeling. The dissociation constant (kd), thermodynamic potential (H) and equilibrium (S) are shown in the table. The negative values of free energy (G) indicate that the reactions were driven enthalpically. The value of n was calculated independently (top left) and then data were fit by fixing n to 7, 14 and 6 (top right, bottom left and bottom right panel, respectively). The arrowheads highlight the poor or no solution for fitting into the independent binding sites model.

Our cryo-EM structure of *Ec*ClpP solved in complex with ADEP1 shows only one axial pore in open conformation. Therefore, it was intriguing to expect at least seven (7) ADEP1 molecules bound to *Ec*ClpP tetradecamer. To test this, we analyzed the data by fixing the number of binding sites to 7 and found that the data could not fit properly into the model (Figure 8). Further, the data fit perfectly into the model once the number of ADEP1 binding sites were fixed to 6. ITC experiments were performed at 25°C. We observed no remarkable difference in results when the experiment was performed at 37°C (data not shown).

3.8 Individually, *Sh*ClpPs did not degrade substrates of different sizes and folded nature

The *S. hawaiiensis* genome encodes six ClpP paralogs instead of only one found in *E. coli* or *B. subtilis.* To understand the mechanism of ADEP1 resistance in *S. hawaiiensis,* we needed to have an assay to measure the hydrolysis rate of ADEP1-activated *Sh*ClpPs. To this end, we assayed the six *Sh*ClpPs against FITC α-casein in the presence of ADEP1. *Ec*ClpP (wt) was used a control in

these experiments and its initial rate was fixed at 100%. We found that none of the six proteins could hydrolyze FITC α-casein (Figure 9A).

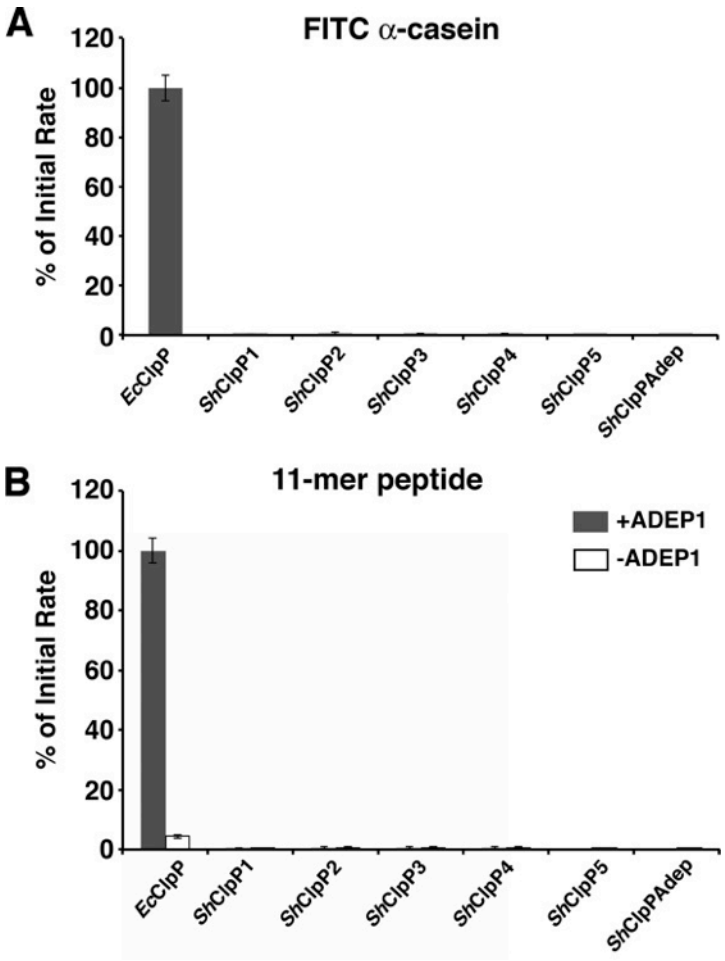

Figure 9: Proteolytic and peptidase activity of *Sh*ClpPs. A. The initial hydrolysis rate of *Sh*ClpP1 through *Sh*ClpP5 and *Sh*ClpPAdep against α-casein. All the reactions were carried out in the presence of ADEP1 to activate ClpP. The initial rates for all *Sh*ClpPs were plotted relative to *Ec*ClpP (wt) that was used a control and its initial rate was said to be 100%. The errors bars represent standard deviation obtained from at least three experimental replicas of each reaction. **B.** The initial rates of *Sh*ClpP1 through *Sh*ClpP5 and *Sh*ClpPAdep against an 11-mer peptide. The data was plotted in the same

We also used an 11-mer peptide as a substrate to test whether *Sh*ClpPs could degrade unfolded substrate of smaller size. Free *Ec*ClpP showed a limited

hydrolysis rate against this substrate, which increased by 20 times in the presence of ADEP1. However, none of the *Sh*ClpPs could degrade this peptide in the absence or presence of ADEP1 (Figure 9B).

Further, we tested the peptidase activity of *Sh*ClpPs against a fluorogenic dipeptide; N-Succinyl-Leu-Tyr-7-amido-4-methylcoumarin (SLY-AMC). This dipeptide can diffuse freely into the catalytic chamber (Thompson *et al.* 1994) bypassing the requirement of ATPases or ADEP1. None of the *Sh*ClpPs could degrade this dipeptide (Table 3).

Table 3. Kinetic parameters of *S. hawaiiensis* ClpPs with Suc-LY AMC peptide.

ClpP **2mM + 10 µM ADEP1**	**Km** **(µM)**	**kcat** **(RFU x s^{-1} $µM^{-1}$)**
*Ec*ClpP (Wild Type)	280 ± 30	8 ± 0.3
*Sh*ClpP1	No peptidase activity	
*Sh*ClpP2	No peptidase activity	
*Sh*ClpP3	No peptidase activity	
*Sh*ClpP4	No peptidase activity	
*Sh*ClpP5	No peptidase activity	
*Sh*ClpPAdep	No peptidase activity	

RFU: Relative Fluorescence Units.

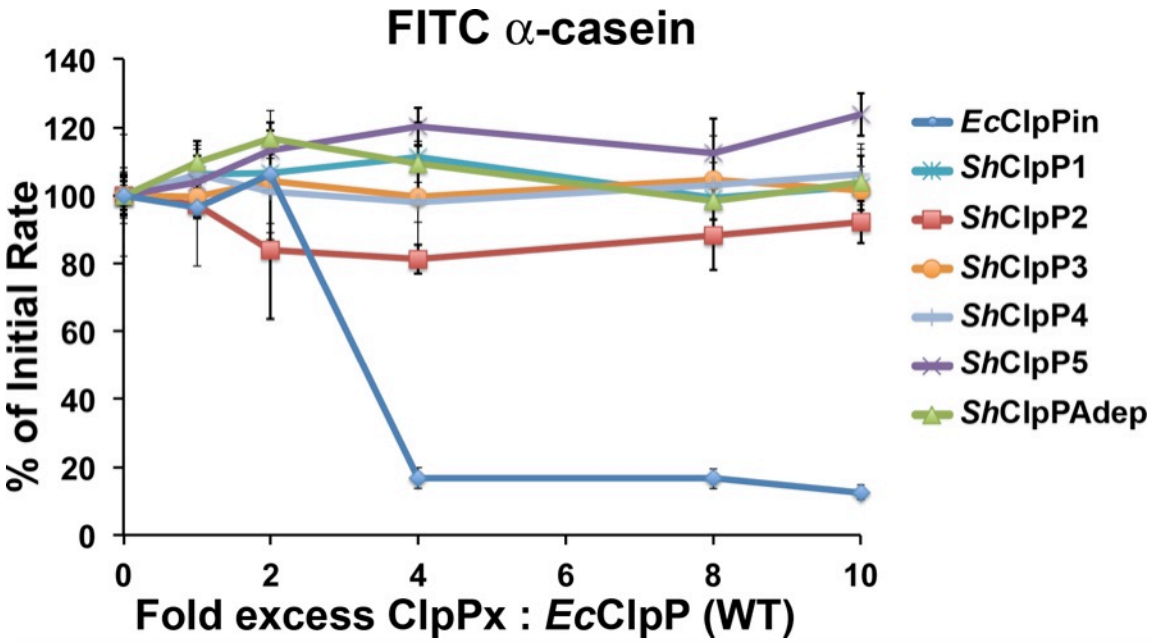

Figure 10: Competition of *Sh*ClpPs with *Ec*ClpP for ADEP1 binding. The hydrolysis rate of -casein by *Ec*ClpP was determined with increasing the concentration of *Sh*ClpPs or *Ec*ClpP$_{in}$ (as control). The initial rate of substrate hydrolysis determined by *Ec*ClpP was defined as 100% and initial rates of each reaction were plotted with respect to it. All the reactions were carried out in the presence of ADEP1. The errors bars represent standard deviation obtained from at least three experimental replicas of each reaction.

3.9 *Sh*ClpPs individually do not bind ADEP1

Next we tested whether *Sh*ClpPs could compete with *E. coli* ClpP for ADEP1 binding. To this end, a fluorescence-based competition assay was performed. In this assay degradation of FITC α-casein by ADEP1-activated wild type *E. coli* ClpP was monitored after adding increasing amount of either individual *Sh*ClpPs or catalytically inactive *Ec*ClpP$_{in}$ as a control (Figure 10).

*Ec*ClpP$_{in}$ cannot degrade FITC α-casein but can sequester ADEP1 from the active wild type *E. coli* CpP, which decreases the initial rate of the reaction. Conversely, if *Sh*ClpPs are unable to compete for ADEP1 will not affect the rate of the reaction when additional amount of the protein is included. Since *E. coli*

ClpP degrades FITC α-casein and none of the *Sh*ClpPs could hydrolyze it, the fluorescence signal can only be attributed to degradation of the substrate by ADEP1-activated wild type *E. coli* ClpP.

We observed that none of the *Sh*ClpPs could compete with *E. coli* ClpP for ADEP1 binding, suggesting that *Sh*ClpPs have significantly lower affinity for ADEP1 as compared to *E. coli* ClpP (Figure 10).

Further, ITC was used to determine whether any of the *Sh*ClpP individually could bind ADEP1. None of the *Sh*ClpPs, showed binding of ADEP1, as indicated by absence of heat release under the effect of exothermal reaction (Figure 11).

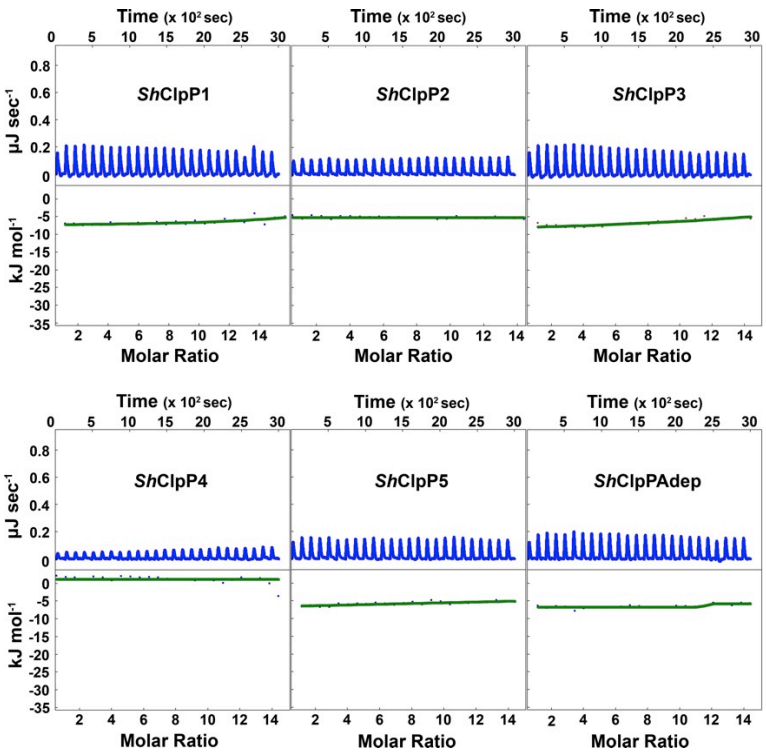

Figure 11: Binding of ADEP1 with *Sh*ClpPs as determined by ITC. ITC data for heat released (blue bars) during titration of *Sh*ClpPs with ADEP1. Small amount of heat released after injecting the ADEP1 into *Sh*ClpPs and absence of a saturation point indicate no binding. A constant and minimal heat released is due to background heat of dilution. A straight line (green) instead of a typical sigmoidal curve (as in Figure 4/5 top left and bottom right panels) indicates no solution for fitting the data into an identical binding site model.

3.10 *Sh*ClpPs did not oligomerize as tetradecamer

We used size exclusion chromatography to determine the oligomeric state of *Sh*ClpPs. In these experiments we needed to have controls representing the size of ClpP tetradecamer and monomer. To this end, wild type *E. coli* ClpP and the N-terminal variant of *B. subtilis* ClpP with glycine substitutions at positions 14 and 15 were used as control. Wild type *E. coli* ClpP eluted at 1.25 ml, corresponding to a tetradecamer of ~300 kDa. The variant of *B. subtilis* ClpP eluted at 1.45 ml, corresponding to monomers of 21.6 kDa. The elution peak of this variant shifted to 1.25 ml, corresponding to the size of a tetradecamer (~300 kDa) in the presence of ADEP1. The oligomeric states of the controls and *Sh*ClpPs were further confirmed by electron microscopy (Figure 12).

All *Sh*ClpPs eluted as one peak (except *Sh*ClpP3 and *Sh*ClpP5) between 1.4-1.55 ml consistent with a monomer of 22-26 kDa. *Sh*ClpP3 and *Sh*ClpP5 appeared mostly as monomer, but with an additional by electron microscopy, these peaks appeared to contain small protein aggregates of heterogeneous morphology (possibly due to freeze-thawing of protein). *B. subtilis* ClpP and its variants do not oligomerize as a tetradecamer, but addition of ADEP1 triggers oligomerization into tetradecamers (Lee *et al.* 2010a). Therefore, we tested whether addition of ADEP1 could induce oligomerization of *Sh*ClpPs. Incubating the proteins with ADEP1 for 15 min triggered a slight shift in the elution peaks of *Sh*ClpP1 and *Sh*ClpP2 towards the tetradecameric peak of *E. coli* ClpP. This subtle change in the elution profile reflected that ADEP1 transformed the monomers of *Sh*ClpP1 and *Sh*ClpP2 to a new oligomeric state. The oligomeric

state of other *Sh*ClpPs remained fairly unaltered in the presence of ADEP1 as indicated by no change in the elution profile and electron microscopy images (Figure 12). Further, incubating *Sh*ClpPs with ADEP1 for 5 hours or overnight did not change the oligomeric state of the proteins (data not shown).

In ITC experiments, we observed that *Sh*ClpP1 and *Sh*ClpP2 do not bind to ADEP1 (Figure 11). However, we noticed a subtle change in the oligomeric state of these proteins by size exclusion chromatography and electron microscopy with ADEP1 (Figure 12). The buffer used in these experiments contained 10% glycerol. Presence of glycerol at this concentration has been reported to trigger oligomerization in ClpP (Lee *et al.* 2010a). Conversely, presence of glycerol at this concentration is not acceptable for ITC experiments (ref. material and methods). Therefore, a glycerol free buffer was used for ITC experiments. The presence of glycerol could be a potential reason for the difference observed in these two sets of experiments. Nevertheless, ADEP1 could not trigger oligomerization to form a tetradecamer in any *Sh*ClpPs.

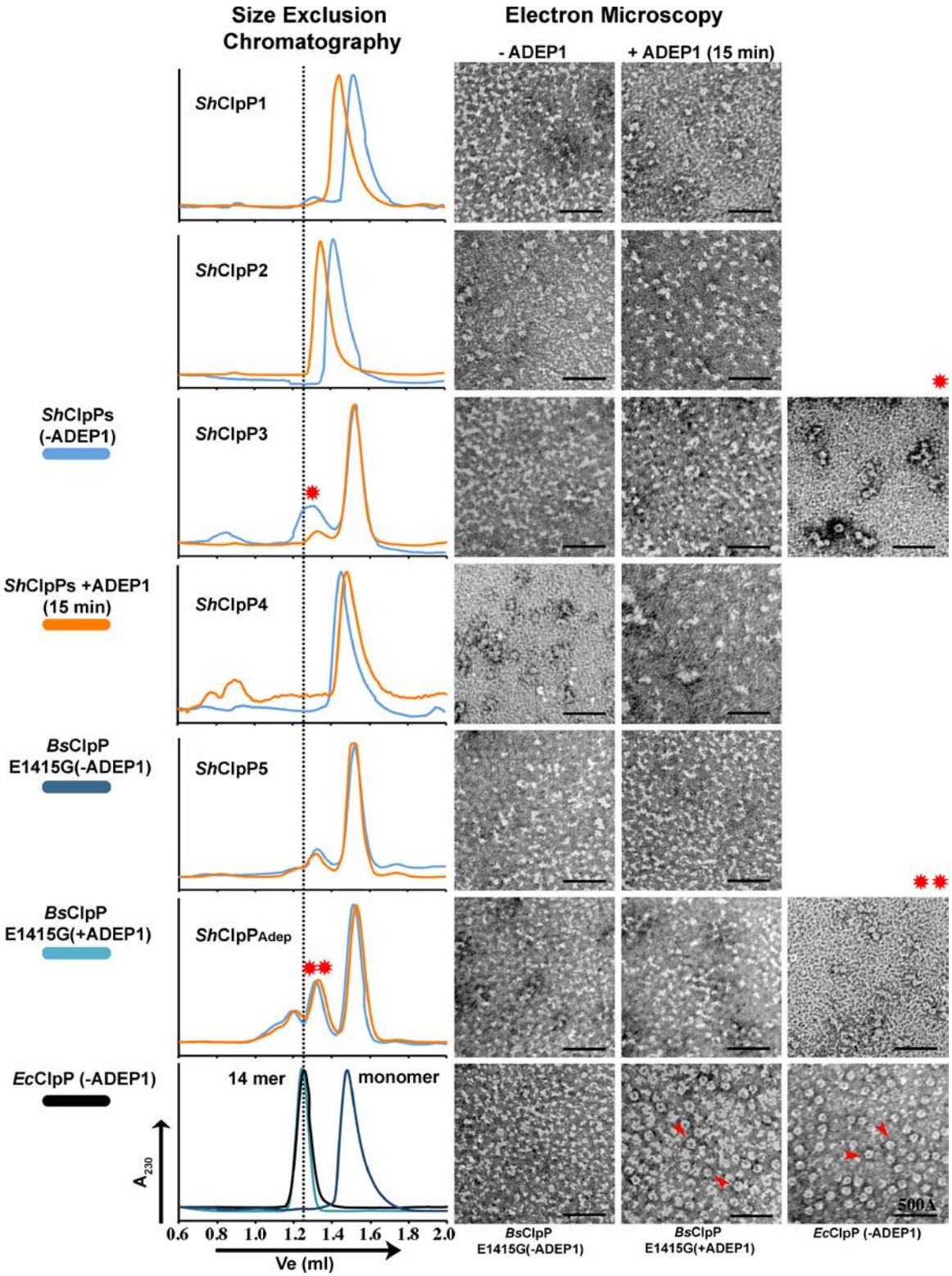
Size Exclusion Chromatography
Electron Microscopy
- ADEP1
+ ADEP1 (15 min)
ShClpP1
ShClpP2
ShClpP3
ShClpP4
ShClpP5
ShClpPAdep
ShClpPs (-ADEP1)
ShClpPs +ADEP1 (15 min)
BsClpP E1415G(-ADEP1)
BsClpP E1415G(+ADEP1)
EcClpP (-ADEP1)
14 mer
monomer
A230
0.6 0.8 1.0 1.2 1.4 1.6 1.8 2.0
Ve (ml)
BsClpP E1415G(-ADEP1)
BsClpP E1415G(+ADEP1)
EcClpP (-ADEP1)
500Å

Figure 12: Oligomeric state of *Sh*ClpPs in the absence and presence of ADEP1. Elution profiles of *Sh*ClpP1 through *Sh*ClpP5 and *Sh*ClpPAdep (top to bottom) were obtained by size exclusion chromatography. Each chromatogram is colored differently according to the sample/experimental conditions. Color scheme of representative curves is shown on the left hand column. The difference in the elution profile among *Sh*ClpPs is due to the difference in their molecular weight that varies from 22 kDa to 26 kDa (monomer). Red asterisks represent the corresponding elution peak or images. The controls are shown in the bottom panel. The dotted line indicates tetradecamer of ~300 kDa. Fractions representing each peak was collected and imaged under electron microscope after performing negative staining (right panel). Arrowheads indicate top views of ClpP rings of *Ec*ClpP and the *B. subtilis* variant.

Streptomyces hawaiiensis clpP1-clpP2 and *clpP3-clpP4* genes are present in bicistronic operons, whereas *clpP5* is alone, and *clpPAdep* is found in the cluster of genes responsible for the synthesis of ADEP1. In *S. lividans*, sensitivity to ADEP1 is dependent on the expression of ClpP1. ClpP1-ClpP2 presumably oligomerize as tetradecamers that are sensitive to ADEP1. In addition, ClpP3-ClpP4 can compensate for the lack of ClpP1 and generate ADEP1 resistance (Gominet *et al.* 2011). *S. lividans* ClpPs (*Sl*ClpPs) have high similarity (>98 - >85%) to their *S. hawaiiensis* homologs. Therefore, it was possible that *Sh*ClpP1-*Sh*ClpP2 and *Sh*ClpP3-*Sh*ClpP4 also form a heteromeric tetradecamer. To test this, equimolar ratios of *Sh*ClpP1 : *Sh*ClpP2 and *Sh*ClpP3 : *Sh*ClpP4 were mixed together and subjected to size exclusion chromatography and electron microscopic imaging. *Sh*ClpP1+*Sh*ClpP2 eluted as a single peak with a shoulder at approximately 1.4 ml, representing the monomeric mixture of these proteins (22 kDa and 25 kDa respectively). Conversely, *Sh*ClpP3+*Sh*ClpP4 eluted as a

double peak between 1.4-1.5 ml, each representing the monomeric state of these proteins (23 kDa and 26 kDa respectively). No remarkable difference in the elution profiles of these proteins was observed when tested in the presence of ADEP1 (Figure 13).

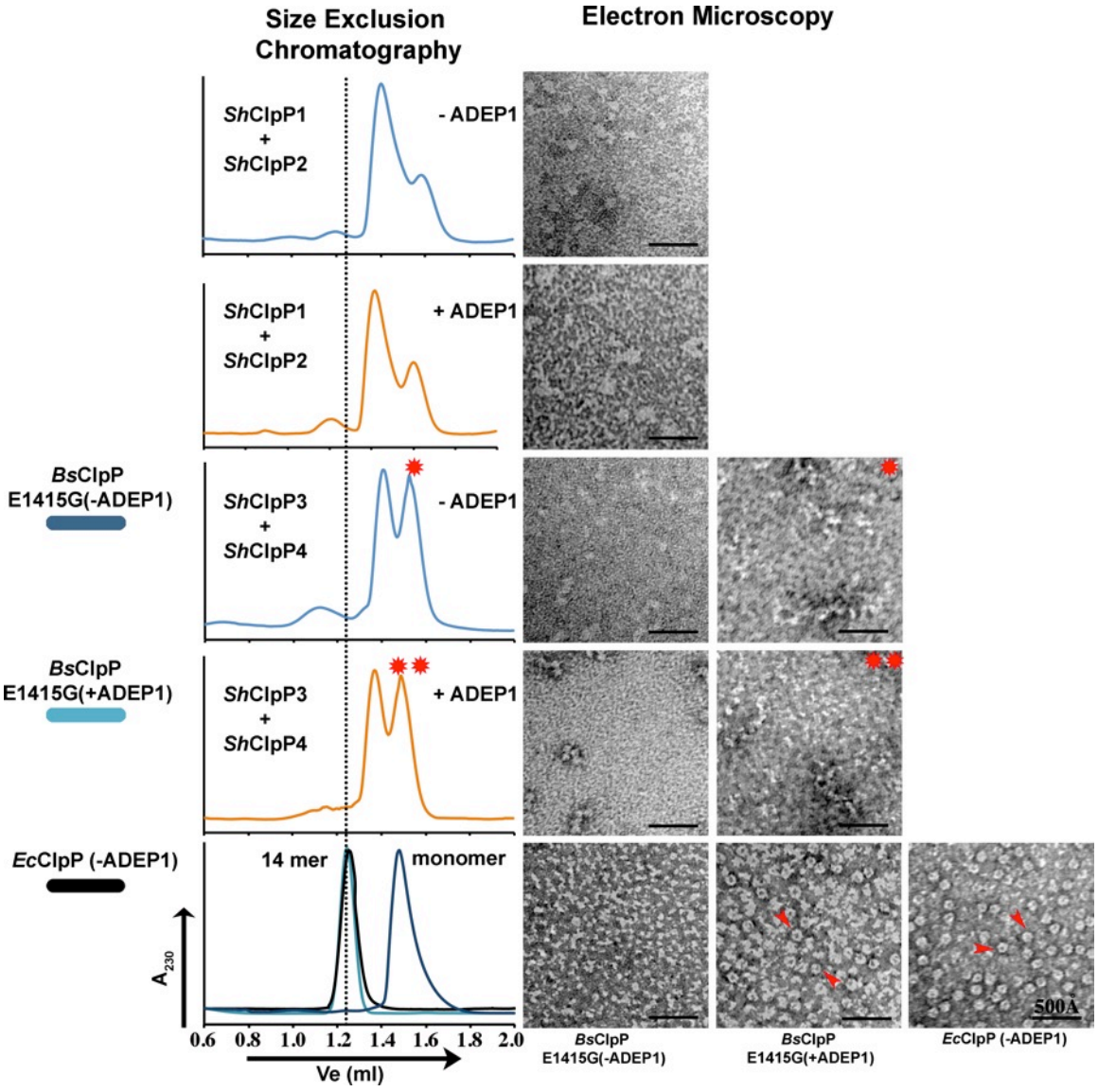

Figure 13: Oligomeric state of bicistronic *Sh*ClpPs.
Figure legends are same as in Figure 12.

Most of the sequenced genomes in *Streptomyces* contain five *clpP* genes with the exception of ClpPAdep, which is an additional gene in *S. hawaiiensis.* Sequence alignments revealed that the hydrophobic pocket required to bind with ADEP1 is not well conserved in *Sh*ClpPAdep as compared to other *Sh*ClpPs (Figure 14).

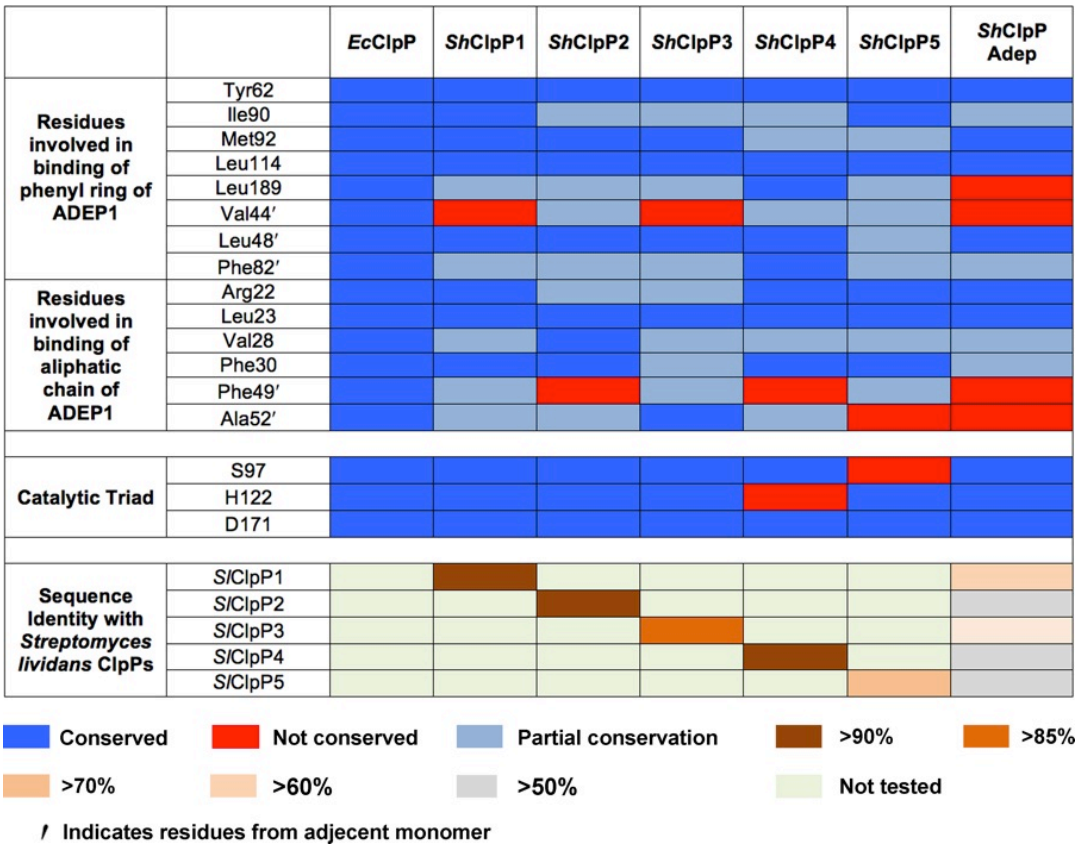

Figure 14: Protein sequence analyses of *S. lividans* and *S. hawaiiensis.* Schematic diagram adopted from the sequence alignment data, representing the conserved hydrophobic cluster required for ADEP1 binding, catalytic triad, and % identity of ClpP proteins. The sequence alignments of *S. hawaiiensis* (NRRL 15010) ClpPs and *S. lividans* (1326) were generated using the sequence alignment tool ClustalW2 (www.ebi.ac.uk/Tools/services/web/toolform.ebi?tool=clustalw2) and percent identities were calculated by pairwise alignment algorithm (www.ebi.ac.uk/Tools/emboss/align/index.html).

It was possible that *Sh*ClpPAdep forms a heteromeric tetradecamer with any of five other *Sh*ClpPs in *S. hawaiiensis,* which is inherently resistant to ADEP1. With the exception of *Sh*ClpP4/5, as the catalytic triad is not conserved in these proteins (Figure 14), any combination with *Sh*ClpPAdep would be catalytically active but resistant to ADEP1. Since ClpP1 and ClpP2 have already been shown to be a functional protease in *S. lividans*, the likely combination of *Sh*ClpP1-*Sh*ClpPAdep or *Sh*ClpP2-*Sh*ClpPAdep to form a heteromeric complex was also tested. Mixtures of these proteins eluted between 1.4-1.55 ml, consistent with the size of their monomers (Figure 15) ruling out the formation of *Sh*ClpP1-*Sh*ClpPAdep or *Sh*ClpP2-*Sh*ClpPAdep to form a heteromeric complexes.

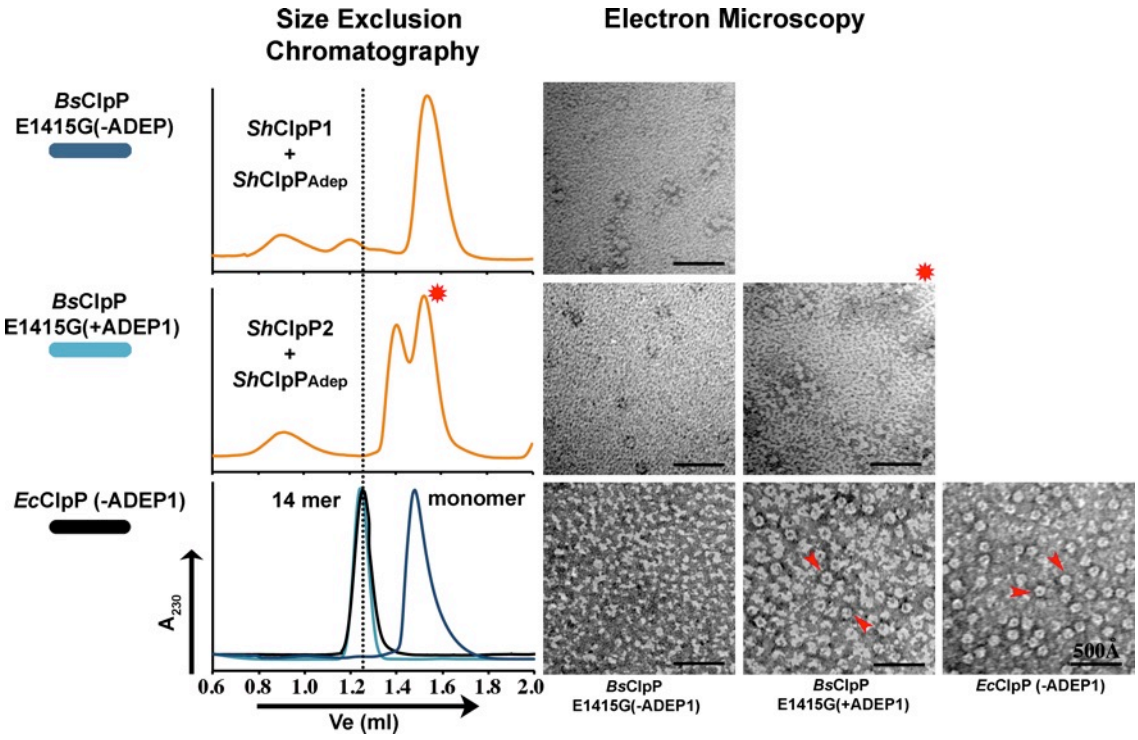

Figure 15: Oligomeric state of heteromeric *Sh*ClpPs. Figure legends are same as in Figure 13.

In conclusion, the results indicated that *Sh*ClpPs do not oligomerize as homomeric or heteromeric-tetradecamer, at least for the tested combinations. Addition of ADEP1 did not cause the proteins to oligomerize and form an active proteolytic catalytic chamber.

Acknowledgement: The *B. subtilis* ClpP variants, ^{8}EQTNRG<u>AA</u>^{15}+<u>A</u>^{25}, ^{8}E<u>GGGGGGG</u>^{15}+K^{25} and ^{8}EQTNRG<u>AA</u>^{15}+ K^{25} were generated, purified and enzymatically tested by Lopamudra Homchaudhuri, (a previous post doctorate fellow of Dr. Joaquin Ortega's lab). She also performed the fluorescence based biochemical assays of these variants and *Sh*ClpP proteins.

4. Discussion

Two opposing models for ADEP1-induced axial gate opening of ClpP have been proposed in *E. coli* (Li *et al.* 2010) and *B. subtilis* (Lee *et al.* 2010a). Both models are based on the X-ray structure of ClpP in complex with ADEP1. The model based on the Li structure (Li *et al.* 2010) proposes that the N-terminal residues of *Ec*ClpP adopt a structured β-hairpin upon ADEP1 binding. This conformation is further stabilized by electrostatic interactions among the charged residues in the N-terminus of ClpP. Conversely, the model based on the Lee structure (Lee *et al.* 2010a) proposes that the N-terminal residues become disordered upon ADEP1 binding, hence are not visible in the X-ray structure. Most of these residues are clearly visible in the Li structure (Li *et al.* 2010) and adopt a β-hairpin conformation without being engaged in crystal contacts. Therefore, this structure provided us ample information to predict the structural determinants that stabilize the open conformation of the axial pores in ClpP. Based on secondary structure predictions, a number of N-terminal variants of *Ec*ClpP were generated. These variants were tested for their ability to translocate substrates of different size to examine the role of predicted structural determinants in stabilization of the axial channel of ClpP.

It was observed that the electrostatic interactions in the N-terminal region have a modest contribution, whereas the integrity of the β-hairpin and the hydrophobic cluster region at its base are essential elements for a functional axial gate. Since, the study was conducted in *E. coli* ClpP, it was unclear whether the mechanism of ADEP1-induced activation of ClpP is conserved in *B. subtilis.*

Herein we have generated equivalent variants in *Bs*ClpP to investigate whether the identified structural determinants in *E. coli* ClpP are also conserved in *B. subtilis* ClpP.

4.1 Mechanism of ADEP1-induced activation of ClpP in *E. coli and B. subtilis*

Our experiments suggest that electrostatic interactions observed in the X-ray structure of *Ec*ClpP in complex with ADEP1 (Li *et al.* 2010) have a modest effect in stabilizing the open conformation of the axial gate. Compromising the ability of N-terminal residues to adopt a structured β-hairpin prevented the translocation of FITC α-casein into the catalytic chamber of *Bs*ClpP (Figure 5A). Consistent with the Li model (Li *et al.* 2010), these results suggest that the ability of N-terminal residues to adopt a "structured β-hairpin" is an essential requirement for the open conformation and efficient translocation of protein substrate into the catalytic chamber of *Bs*ClpP (Figure 5A). The N-terminal residues of ClpP are observed to adopt a β-hairpin conformation in the crystal structures of ADEP1-free ClpP from other organisms, for example, *Coxiella burnetii* (PDB 3Q7H) and *S. aureus* (Zhang *et al.* 2011). Furthermore, the flexibility in the N-terminal region compromised the ability of the axial gate to translocate FITC α-casein into the catalytic chamber of ClpP (Figure 5A). These findings are in direct contrast with the model proposed from crystal structure of the *B. subtilis* ClpP in complex with ADEP1 (Lee *et al.* 2010a). Our results implied that the increased flexibility of the N-terminal region proposed by the Lee model

(Lee *et al.* 2010a) is a consequence of crystal packing rather than ADEP1 binding. These results are in agreement with the results for *E. coli* ClpP.

When tested against the an 11-mer peptide, the variants with substitution of N-terminal charged residues (Glu14, Arg15 and Lys25) by alanine or glycine showed almost comparable hydrolysis rates to that of wild type *Bs*ClpP. It could be inferred that the charged residues are not essential for the conformation required to translocate an 11-mer peptide. Instead, we see these results in a different perspective. Though unfolded, this peptide is too large to be translocated through axial pore of ClpP when the pore is in closed conformation. Therefore, ADEP1 is required to open the axial channel for efficient translocation and degradation of this substrate. The equivalent variants of *E. coli* ClpP have a 2-20 times higher hydrolysis rate for the 11-mer peptide compared to that of wild type, even in the absence of ADEP1. Addition of ADEP1 resulted in an additional increase in the hydrolysis rate for the variants. It was concluded that the charged residues contribute to the stabilization of the closed conformation of the axial gate. Wild type *B. subtilis* ClpP and its variants are dependent on ADEP1 for oligomerization. Therefore, it was not possible to test the role of charged residues in the closed conformation of axial channel. However, we found similar hydrolysis rates when compared with the results obtained from ADEP1-activated variants of *Ec*ClpP. We interpret the results of hydrolysis rates of an 11-mer peptide in the context of the results obtained by their counterpart variants in *E. coli*. Based on the above discussion, we conclude that the charged residues in the N-terminus of

ClpP contribute in maintaining the closed conformation of the axial gate in *B. subtilis*.

Consistent with the observation in *E. coli* (Alexopoulos *et al.* 2013) the data presented here show that structural determinants required for the open conformation of the axial gate to translocate large unfolded substrate (FITC α-casein) are not the same for substrates of small size (11-mer peptide). Large and unfolded substrates need an efficient enzymatic processivity; therefore, we infer that formation of the structured β-hairpin is a contribution towards ClpP processivity.

An important caveat while considering the conserved nature of gating mechanism in these bacteria is that the role of the hydrophobic cluster region at the base of the β-hairpin could not be investigated in *B. subtilis* ClpP. Compromising the hydrophobic cluster in *B. subtilis* ClpP hinders the oligomerization of *Bs*ClpP as a tetradecamer (Lee *et al.* 2010a). This posed a limitation to test the role of this structural element in stabilizing the open conformation of the axial channel. Compromising the hydrophobic cluster in *E. coli* ClpP variant (Alexopoulos *et al.* 2013) hindered the ability of FITC α-casein to access the catalytic chamber, which contrasts with the model based on the X-ray structures of *B. subtilis* ClpP in complex with ADEP1 (Lee *et al.* 2010a). *E. coli* and *B. subtilis* ClpP share 77% sequence identity among N-terminal residues (first 25 amino acids) and protomers of 3TT7 and 1TYF can be superimposed with an root mean square deviation (rmsd) of 0.56 Å (Alexopoulos *et al.* 2013).

Further, structural comparison has revealed the existence of an identical hydrophobic cluster region in *E. coli* and *B. subtilis* ClpP (Alexopoulos *et al.* 2012). Therefore, it is unlikely that role of the hydrophobic cluster region in stabilizing the axial channel is different in *E. coli* and *B. subtilis* ClpP.

The biochemical and structural work conducted by generating the equivalent variants of conserved amino acids in *E. coli* (Alexopoulos *et al.* 2013) and *B. subtilis* ClpP (herein) suggest that the ADEP1 induced gating mechanism is conserved in these bacteria.

4.2 Conformation of the ADEP1-bound *Ec*ClpP

Our 3D cryo-EM structure suggests that ADEP1-bound *Ec*ClpP adopts a different conformation in solution than observed the X-ray structure (Li *et al.* 2010). Specifically, the asymmetric axial regions and side pores are not observed in the X-ray structure of ADEP1-bound ClpP. Though not common, the asymmetric nature of free ClpP has been observed in the X-ray crystal structure of free *Ec*ClpP (Bewley *et al.* 2006) and also in the three-dimensional cryo-EM structure of ClpA-bound *Ec*ClpP (Effantin *et al.* 2010b). Our data shows an asymmetric nature of the axial regions both in free and ADEP1-bound ClpP. The study of *Ec*ClpP using HDX-MS suggests a dynamic nature of the axial region of ADEP1-activated ClpP (Sowole *et al.* 2013). The authors attributed the accelerated HDX in the axial region of ADEP1-activated ClpP to the dynamic nature of the β-hairpin adopted by the N-terminal residues and a conformational change due to the hydrophobic pull exerted by ADEP1 in the N-terminal region

(Sowole *et al.* 2013). The results here suggest that increased HDX rate may be attributed more to the dynamic behavior of axial regions, rather than flexibility of the β-hairpin.

The second noticeable difference in the cryo-EM structure of ADEP1 bound *Ec*ClpP is the presence of side pores. Contrary to the compressed states of ClpP, our cryo-EM data show that the side pores are slightly off the equatorial belt and contained exclusively within one heptamer. This heptamer also an lacks axial channel in the open conformation. Being asymmetric in nature, it is possible that the two heptamers of ClpP perform different functions during proteolysis. The heptamer with side pores and a closed axial channel might represent the compressed state meant for product release. Conversely, the opposite heptamer with an open axial channel might be in the extended conformation and engaged in translocating substrate to the catalytic chamber.

Earlier NMR work (Sprangers *et al.* 2005) proposed that side pores are transiently formed in the equatorial region for product release. Contrary to the NMR data, the pronounced stabilization of the equatorial region seen in HDX-MS argues for rigid nature of the equatorial region (Sowole *et al.* 2013). It is important to note that the NMR data obtained in the study (Sprangers *et al.* 2005) were interpreted in the favor of a model where the degradation products are released from ClpX/A-ClpP complex. However, the study using HDX-MS (Sowole *et al.* 2013) was conducted on free and ADEP1-bound ClpP, a situation identical to our

study. Therefore, we interpret the cryo-EM data in the context of the HDX-MS results.

Overall, our cryo-EM structure of ADEP1-bound *Ec*ClpP contrasts with the published X-ray structures of ClpP solved in the presence of ADEP1 (Lee *et al.* 2010a) (Li *et al.* 2010). These structures show symmetrical heptamers of ClpP with two axial gates in the open conformation and an absence of side pores. One possible explanation of these differences could be that ADEP1 binds to only one end of ClpP and triggers a signal to the opposite end, preventing further ADEP1 binding. It is also possible that in solution, ADEP1 binds to both ends of ClpP but opens only one axial gate. Both of these models point towards an allosteric signal mechanism involved in the activation of ClpP upon ADEP1 binding. It is possible that crystal contacts in the X-ray structures blocked the propagation of these allosteric signals, generating a crystal structure different from the protein conformation existing in solution.

4.3 Stoichiometry of ADEP1: *Ec*ClpP

Analysis of ITC data under different conditions supported that only 6 molecules of ADEP1 were bound to *Ec*ClpP in solution (Figure 8). Indeed, these results not only complemented the asymmetry observed in cryo-EM structure but also were physiologically relevant as ClpP's ATPases; ClpX and ClpA have six IGF/L loops to bind with ClpP. The quantitative unit of affinity, dissociation constant (K_d) = 0.33 ± 0.04 μM, measured in this study is comparable to the published data (Leung *et al.* 2011). On the other hand, the number of binding

sites contrast (n = 6 versus 14) with the results published in the same study. This could be due to the difference in the temperatures (25°C versus 37°C) at which the experiments were performed. In this context, we repeated the experiments at 37°C. Similar results were obtained at 37°C, indicating that temperature was not a contributing factor towards this difference.

Contrary to the X-ray structure of ADEP1-bound *Ec*ClpP (Li *et al.* 2010), our cryo-EM structure of *Ec*ClpP in complex with ADEP1, and ITC data, show that ADEP1 triggers opening of only one axial pore and a maximum of 6 molecules of ADEP1 can bind to *Ec*ClpP. These results suggest that the conformation adopted by *Ec*ClpP upon ADEP1 binding, and the stoichiometric ratio of antibiotic to ClpP tetradecamer is different than what is observed in the X-ray structure (Li *et al.* 2010). Could these differences be attributed to the distinct conditions of crystalline versus solution environment? The X-ray structures elegantly provide a snapshot of a protein at the atomic level; however, the non-physiological environment of crystallization can induce conformational changes that are not inherent to the protein. A member of the Clp family of ATPase, HslU exemplifies this scenario. *E. coli* HslU is a hexameric ATPase that binds coaxially with its double hexameric protease unit of HslV to form an ATP-dependent bacterial protease complex, HslVU (also called ClpYQ) (Rohrwild *et al.* 1996) (Yoo *et al.* 1996). The crystal structure of HslVU showed that the I-domains of HslU protrude out from its small ring and bind with HslV (Bochtler *et al.* 2000). This complex, when preserved fully hydrated and close to the physiological state

of cryo-electron microscopy, revealed a quite different orientation of how HslU binds with HslV. According to the cryo-EM structure based model, the I-domains of HslU protrude distally and are involved in substrate recognition rather than binding with HslV. Instead, the ATPase domain of the wider and denser ring of HslU contacts the protease HslV (Ishikawa *et al.* 2000). Based on the above discussion we attribute the differences in dynamic behavior, conformation and stoichiometry of ADEP1 to ClpP to the difference of the solution versus crystalline environment of the experiments.

4.4 Our current model of ClpP activation

Given that a maximum of 6 molecules of ADEP1 can bind to *Ec*ClpP, as observed in ITC experiments, it is possible that ADEP1 only binds to the heptamer with an extended conformation and triggers opening of the axial channel in this heptamer. The second conformational change in the opposite heptameric ring may be induced by an allosteric signal, triggered by ADEP1 binding. This change might create side pores for product release and disrupt the hydrophobic pockets on the axial surface to prevent further binding of ADEP1. This extended-compressed hybrid model explains the simultaneous activation of ClpP by opening of the axial gate and release of degradation products through side pores.

Could this model explain the symmetry mismatch between hexameric ATPases and heptameric ClpP? Different models have been proposed to address the symmetry mismatch between the ATPases and ClpP (Beuron *et al.*

1998, Bewley *et al.* 2006, Effantin *et al.* 2010a, Martin *et al.* 2007). Biochemical studies established that all six IGF/L loops of ATPase hexamer are essential for the binding with ClpP (Martin *et al.* 2007). Therefore, we assume that the conformation changes required to accommodate the symmetry mismatch between ATPase and ClpP would be contributed mainly by ClpP. Since ADEP1 mimics IGF/L loops of ClpX/A, it can be deduced that only six N-termini of the ClpP heptamer are involved in interaction with the ATPase. This model helps to explain the symmetry mismatch only in 1:1 ATPase- ClpP complexes but is unable to explain 2:1 complexes that would need 12 hydrophobic pockets of ClpP to be occupied by IGF/L or ADEP1. ADEP1 mimics the IGF/L loops of the ATPase but still lacks its pore 2 loop interactions with N-terminus of ClpP. Though these interactions are relative weaker, dynamic and vary with the nucleotide state, they are still important for ClpP binding (Bewley *et al.* 2006, Martin *et al.* 2007, Bewley *et al.* 2006). It is possible that the IGF/L and pore-2 loop interactions synergistically provide enough strength for these proteins to interact as 2:1 complexes of ClpX/A-ClpP. In such a case, the ATPase would activate one heptameric ring of ClpP at a given time. A structural study (Ortega *et al.* 2002) conducted on 2:1 ClpXP complex supports this possibility, showing that substrate is alternatively translocated through the axial pores into the catalytic chamber of ClpP. Alternatively, it is also possible that the ATPases bind to each end of ClpP in sub-stoichiometric ratio, e.g 3 IGF/L loops per heptamer of ClpP, to form a 2:1 ATPase-ClpP complex.

Side pores were not observed in the cryo-EM structure of ClpAP (1:1) complex (Effantin *et al.* 2010b), indicating that equatorial region of *Ec*ClpP might respond differently when activated by ClpA. Several other studies in *S. aureus*, *B. subtilis,* and *E. coli* ClpP (Kimber *et al.* 2010, Lee *et al.* 2011, Ye *et al.* 2013) have also proposed the presence of side pores in the vicinity of equatorial region. These studies propose that small fluctuations in the handle region and conformational switching between extended and compressed state triggers the generation of side pores next to the active site. A recent study has proposed that a steric bulk at the active site, or native peptides with large side chains exposed during the transition from extended to compressed state may trigger such a switch to generate side pores (Gersch *et al.* 2014). Our extended-compressed hybrid model does not support such conformational switching of ClpP tetradecamers between extended and compressed states. Rather, it favors allosterically induced extended and compressed states of heptamers in same tetradecamer.

4.5 Mechanism of ADEP1 self-resistance in *S. hawaiiensis*

ADEP1 is not only a useful tool to understand the nature of the ClpX/A-ClpP complex (Gominet *et al.* 2011, Sass *et al.* 2011, Lee *et al.* 2010a, Li *et al.* 2010) but also proved to be an effective antibiotic (Schiefer *et al.* 2013). However, the mechanism of ADEP1 self-resistance in *S. hawaiiensis* is still unknown. Our initial attempts to address this question could only provide the information that *Sh*ClpPs did not oligomerize as tetradecamer, even the presence

of ADEP1 could not induce oligomerization as seen in *B. subtilis* ClpP. Further, none of the *Sh*ClpPs showed binding to ADEP1. Without identifying a functional ClpP protease in *S. hawaiiensis,* we cannot conclude that “no affinity for ADEP1” is the mechanism of self-resistance.

Most of our knowledge about ADEP1 resistance in *Streptomyces* comes from a recent study of *S. lividans*, (Gominet *et al.* 2011). In this bacterium, *Sl*ClpP1 and *Sl*ClpP2 are constitutively expressed and control the expression of *Sl*ClpP3 and *Sl*ClpP4 by degrading its activator, PopR. Therefore *Sl*ClpP3 and *Sl*ClpP4 are not expressed in wild type. However, mutation of *Sl*ClpP1 gene allowed for expression of *Sl*ClpP3 and contributed towards ADEP1 resistance in *S. lividans.* Although there is no direct evidence, the study suggests that *Sl*ClpP1-*Sl*ClpP2 and *Sl*ClpP3-*Sl*ClpP4 might form heteromeric tetradecamers, where the latter compensate for the inhibition of the former complex and contribute towards ADEP1 resistance. Based on high sequence identity (>98-85%) of these proteins and bicistron arrangement of the *shclP* genes, it was possible that *Sh*ClpP1-*Sh*ClpP2 and *Sh*ClpP3-*Sh*ClpP4 also form heteromeric tetradecamers, where the former is sensitive but the latter resistant to ADEP1. Given that *Sh*ClpP4 lacks canonical catalytic triad, it was important to consider that the heteromeric complex of *Sh*ClpP3-*Sh*ClpP4 could be catalytically inactive. However, it has been established that ClpP3-ClpR of *Synechococcus* (Andersson *et al.* 2009) and the eukaryotic 20S proteasome core complex are catalytically active despite having inactive ClpR and α-subunits in their heteromeric complexes. Such

heteromeric complexes have been proposed to play a crucial role in association of the core complex with the ATPase subunits (Andersson *et al.* 2009).

The presence of paralogues in *Streptomyces* is usually explained as allowing selective expression during different phases of bacterial life (Gominet *et al.* 2011). Similar to the duplication of *clpP operons in S. hawaiiensis* and *S. lividans, Streptomyces griseus* has two genes for tryptophanyl-tRNA synthetase. One of the genes codes for the enzyme sensitive to indolmycin, which is an antibiotic produced by the same bacteria. Upon the production of the antibiotic, the second gene is expressed that encodes an enzyme that is resistant to the antibiotic (Vecchione and Sello 2009). It was tempting to speculate such an "alternative gene expression" as the mechanism of ADEP1 resistance in *S. hawaiiensis* as well. We hypothesized that *Sh*ClpP1-*Sh*Clp2 is the functional proteolytic unit in *S. hawaiiensis*, which is sensitive to ADEP1. However, upon ADEP1 production, *Sh*ClpPAdep is "alternatively expressed" and replaces either of these *Sh*ClpPs to form a heteromeric-ClpP complex, which is resistant to the antibiotic. Herein, we tested both of the above-mentioned models that could possibly elucidate the ADEP1 resistance mechanism in *S. hawaiiensis.* The data could not support either, simply because of inability of *Sh*ClpPs to oligomerize as heteromeric tetradecamer. Unlike *clpP1clpP2* and *clpP3clpP4, the clpP5* gene is not present in bicistronic arrangement, therefore *Sh*ClpP5 was not tested for any heteromeric combinations.

An important caveat while considering these results is that the interaction of *Sh*ClpPs with their cognate ATPases was not addressed in these experiments. Although, ADEP1 mimics the IGF/L loops of ATPase, it might not necessarily induce oligomerization, as would ATPases in *S. hawaiiensis*. In the situation where the complete genome of *S. hawaiiensis* has not yet been annotated and the cognate ATPase genes are not available, ATPase of other bacterial origin can be used to examine whether they can induce oligomerization in *Sh*ClpPs. Human ClpP oligomerizes upon association with *E. coli* ClpX. This ATPase-protease hybrid complex successfully adopted the substrate specificity of ClpX as well (Kang *et al.* 2004). Therefore, the effects of ATPases on the oligomeric states of *Sh*ClpPs could possibly be examined using ATPase foreign origin.

A bicistronic arrangement of *clpP* genes is also present in the Cyanobacterium *Synechococcus,* where *clpP3* and *clpR* genes are arranged within a bicistronic operon (Schelin, Lindmark and Clarke 2002). Clp3 and ClpR form a heteromeric complex in this bacterium. A similar approach, that we have used to assemble a heteromeric *Sh*ClpPs, failed to reconstitute ClpP3/ClpR by mixing the purified proteins. However, the heteromeric complex was successfully obtained by co-expressing the genes in the same cell using an *E. coli* expression system (Andersson *et al.* 2009). Likewise, purification of recombinant proteins or affinity based purification of heteromeric complex from cell lysate would be helpful to identify the heteromeric complex of *Sh*ClpPs. ClpPs of *S. hawaiiensis* and *S. lividans* share high sequence identity. It is unlikely that the ClpP functional

protease complex in these bacteria would be different. Given that *clpPAdep* gene is only the additional gene in *S. hawaiiensis,* its transfer into *S. lividans* may also provide a useful approach to probe the mechanism of ADEP1 immunity in *S. hawaiiensis.*

An N-terminal signal peptide of 14 residues is present in *E. Coli* ClpP, which is subsequently cleaved by bacterial proteases. Since the *S. hawaiiensis* ClpPs were expressed in *E. coli* system, it is possible that the N-terminal signal peptides of 14 and 12 residues in *Sh*ClpP1 and *Sh*ClpP2, respectively, are not processed, and thus hindered oligomerization. Other *Sh*ClpPs and homologous proteins in *S. lividans* lack these pro-peptide sequences (Figure 16). Cleaving these pro-peptide sequences and testing for the oligomeric state would be a promising approach for future studies in order to elucidate the physiological ClpP protease complex and eventually ADEP1 resistance in *S. hawaiiensis.* Although we are unable to reveal the ADEP1 resistance mechanism, these results constitute the biochemical and structural characterization of previously undescribed proteins.

In addition to target substitution, the SclAB efflux pump and other still uncharacterized mechanisms are also reported to be responsible for ADEP1 resistance in *S. lividans* (Gominet *et al.* 2011). In this context, our lab is collaborating with Dr. Broetz-Oesterhelt's laboratory (Universität Düsseldorf, Germany) to carry out *in vivo* studies for the identification of other mechanisms potentially involved in ADEP1 resistance in *S. hawaiiensis.*

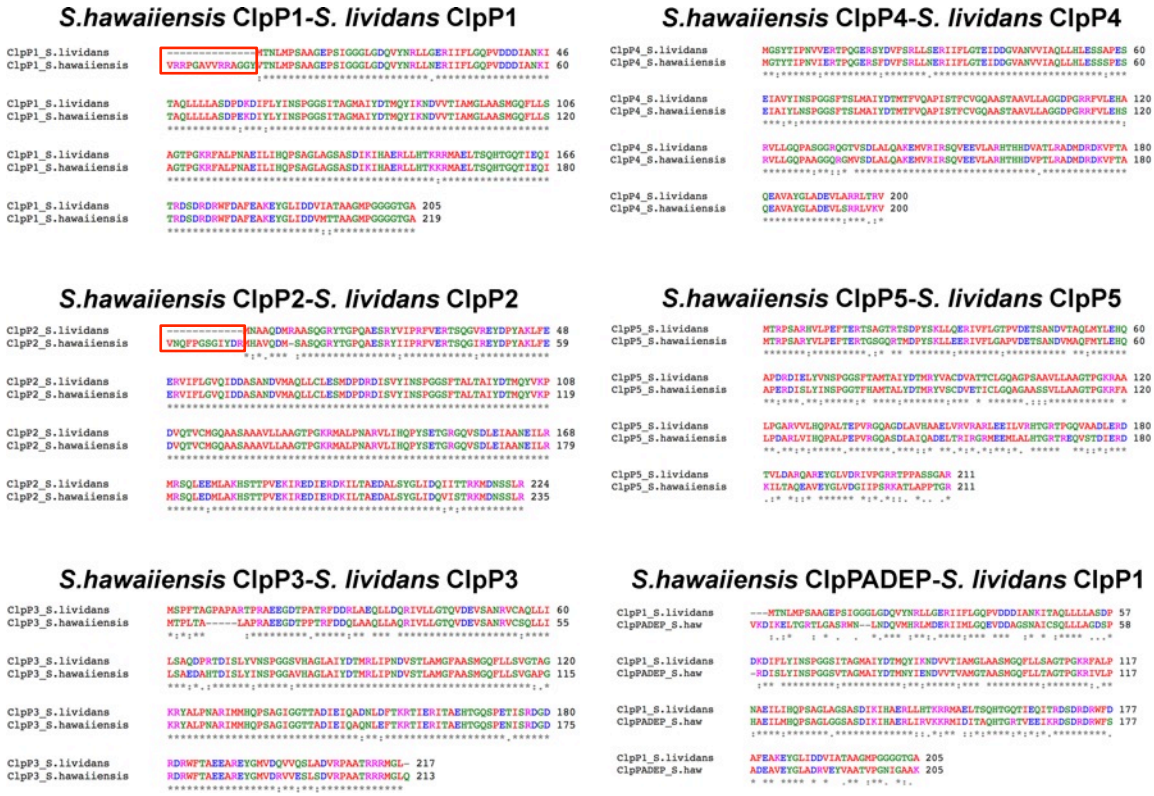

Figure 16: Sequence alignments of *S. hawaiiensis* and *S. lividans* ClpPs. The alignment files were generated using the sequence alignment tool ClustalW2 (www.ebi.ac.uk/Tools/services/web/toolform.ebi?tool=clustalw2). The red boxes indicate the overhung non-overlapping pro-peptide sequences of *Sh*ClpP1 and *Sh*ClpP2. On the basis of highest sequence identity (>70 %) as compared to others *Sh*ClpPAdep is aligned with ClpP1 of *S. lividans*.

Together, these results are broadening our understanding on ClpP activation and also the resistance mechanism against this class of antibiotics.

5. References

Alexopoulos, J., B. Ahsan, L. Homchaudhuri, N. Husain, Y. Q. Cheng & J. Ortega (2013) Structural determinants stabilizing the axial channel of ClpP for substrate translocation. *Mol Microbiol,* 90**,** 167-80.

Alexopoulos, J. A., A. Guarne & J. Ortega (2012) ClpP: a structurally dynamic protease regulated by AAA+ proteins. *J Struct Biol,* 179**,** 202-10.

Andersson, F. I., A. Tryggvesson, M. Sharon, A. V. Diemand, M. Classen, C. Best, R. Schmidt, J. Schelin, T. M. Stanne, B. Bukau, C. V. Robinson, S. Witt, A. Mogk & A. K. Clarke (2009) Structure and function of a novel type of ATP-dependent Clp protease. *J Biol Chem,* 284**,** 13519-32.

Baker, T. A. & R. T. Sauer (2006) ATP-dependent proteases of bacteria: recognition logic and operating principles. *Trends Biochem Sci,* 31**,** 647-53.

Bellier, A., M. Gominet & P. Mazodier (2006) Post-translational control of the *Streptomyces lividans* ClgR regulon by ClpP. *Microbiology,* 152**,** 1021-7.

Beuron, F., M. R. Maurizi, D. M. Belnap, E. Kocsis, F. P. Booy, M. Kessel & A. C. Steven (1998) At sixes and sevens: characterization of the symmetry mismatch of the ClpAP chaperone-assisted protease. *J Struct Biol,* 123**,** 248-59.

Bewley, M. C., V. Graziano, K. Griffin & J. M. Flanagan (2006) The asymmetry in the mature amino-terminus of ClpP facilitates a local symmetry match in ClpAP and ClpXP complexes. *J Struct Biol,* 153**,** 113-28.

Bochtler, M., C. Hartmann, H. K. Song, G. P. Bourenkov, H. D. Bartunik & R. Huber (2000) The structures of HsIU and the ATP-dependent protease HsIU-HsIV. *Nature,* 403**,** 800-5.

Brotz-Oesterhelt, H., D. Beyer, H. P. Kroll, R. Endermann, C. Ladel, W. Schroeder, B. Hinzen, S. Raddatz, H. Paulsen, K. Henninger, J. E. Bandow, H. G. Sahl & H. Labischinski (2005) Dysregulation of bacterial proteolytic machinery by a new class of antibiotics. *Nat Med,* 11**,** 1082-7.

Choi, K. H. & S. Licht (2005) Control of peptide product sizes by the energy-dependent protease ClpAP. *Biochemistry,* 44**,** 13921-31.

Effantin, G., T. Ishikawa, G. M. De Donatis, M. R. Maurizi & A. C. Steven (2010a) Local and global mobility in the ClpA AAA+ chaperone detected by cryo-electron microscopy: functional connotations. *Structure,* 18**,** 553-62.

Effantin, G., M. R. Maurizi & A. C. Steven (2010b) Binding of the ClpA unfoldase opens the axial gate of ClpP peptidase. *J Biol Chem,* 285**,** 14834-40.

El Bakkouri, M., S. Rathore, C. Calmettes, A. K. Wernimont, K. Liu, D. Sinha, M. Asad, P. Jung, R. Hui, A. Mohmmed & W. A. Houry Structural insights into the inactive subunit of the apicoplast-localized caseinolytic protease complex of *Plasmodium falciparum*. *J Biol Chem,* 288**,** 1022-31.

Feng, J., S. Michalik, A. N. Varming, J. H. Andersen, D. Albrecht, L. Jelsbak, S. Krieger, K. Ohlsen, M. Hecker, U. Gerth, H. Ingmer & D. Frees (2012) Trapping and proteomic identification of cellular substrates of the ClpP protease in *Staphylococcus aureus*. *J Proteome Res,* 12**,** 547-58.

Flynn, J. M., S. B. Neher, Y. I. Kim, R. T. Sauer & T. A. Baker (2003) Proteomic discovery of cellular substrates of the ClpXP protease reveals five classes of ClpX-recognition signals. *Mol Cell,* 11**,** 671-83.

Geiger, S. R., T. Bottcher, S. A. Sieber & P. Cramer (2011) A conformational switch underlies ClpP protease function. *Angew Chem Int Ed Engl,* 50**,** 5749-52.

Gersch, M., R. Kolb, F. Alte, M. Groll & S. A. Sieber (2014) Disruption of oligomerization and dehydroalanine formation as mechanisms for ClpP protease inhibition. *J Am Chem Soc,* 136**,** 1360-6.

Gominet, M., N. Seghezzi & P. Mazodier (2011) Acyl depsipeptide (ADEP) resistance in *Streptomyces*. *Microbiology,* 157**,** 2226-34.

Gribun, A., M. S. Kimber, R. Ching, R. Sprangers, K. M. Fiebig & W. A. Houry (2005) The ClpP double ring tetradecameric protease exhibits plastic ring-ring interactions, and the N termini of its subunits form flexible loops that are essential for ClpXP and ClpAP complex formation. *J Biol Chem,* 280**,** 16185-96.

Grimaud, R., M. Kessel, F. Beuron, A. C. Steven & M. R. Maurizi (1998) Enzymatic and structural similarities between the *Escherichia coli* ATP-dependent proteases, ClpXP and ClpAP. *J Biol Chem,* 273**,** 12476-81.

Gur, E., D. Biran & E. Z. Ron (2011) Regulated proteolysis in Gram-negative bacteria--how and when? *Nat Rev Microbiol,* 9**,** 839-48.

Ishikawa, T., F. Beuron, M. Kessel, S. Wickner, M. R. Maurizi & A. C. Steven (2001) Translocation pathway of protein substrates in ClpAP protease. *Proc Natl Acad Sci U S A,* 98**,** 4328-33.

Ishikawa, T., M. R. Maurizi, D. Belnap & A. C. Steven (2000) Docking of components in a bacterial complex. *Nature,* 408**,** 667-8.

Kang, S. G., M. R. Maurizi, M. Thompson, T. Mueser & B. Ahvazi (2004) Crystallography and mutagenesis point to an essential role for the N-terminus of human mitochondrial ClpP. *J Struct Biol,* 148**,** 338-52.

Kessel, M., M. R. Maurizi, B. Kim, E. Kocsis, B. L. Trus, S. K. Singh & A. C. Steven (1995) Homology in structural organization between *E. coli* ClpAP protease and the eukaryotic 26 S proteasome. *J Mol Biol,* 250**,** 587-94.

Kim, Y. I., I. Levchenko, K. Fraczkowska, R. V. Woodruff, R. T. Sauer & T. A. Baker (2001) Molecular determinants of complex formation between Clp/Hsp100 ATPases and the ClpP peptidase. *Nat Struct Biol,* 8**,** 230-3.

Kimber, M. S., A. Y. Yu, M. Borg, E. Leung, H. S. Chan & W. A. Houry (2010) Structural and theoretical studies indicate that the cylindrical protease ClpP samples extended and compact conformations. *Structure,* 18**,** 798-808.

Kirstein, J., A. Hoffmann, H. Lilie, R. Schmidt, H. Rubsamen-Waigmann, H. Brotz-Oesterhelt, A. Mogk & K. Turgay (2009) The antibiotic ADEP reprogrammes ClpP, switching it from a regulated to an uncontrolled protease. *EMBO Mol Med,* 1**,** 37-49.

Langklotz, S., U. Baumann & F. Narberhaus (2011) Structure and function of the bacterial AAA protease FtsH. *Biochim Biophys Acta,* 1823**,** 40-8.

Lee, B. G., M. K. Kim & H. K. Song (2011) Structural insights into the conformational diversity of ClpP from *Bacillus subtilis. Mol Cells,* 32**,** 589-95.

Lee, B. G., E. Y. Park, K. E. Lee, H. Jeon, K. H. Sung, H. Paulsen, H. Rubsamen-Schaeff, H. Brotz-Oesterhelt & H. K. Song (2010a) Structures of ClpP in complex with acyldepsipeptide antibiotics reveal its activation mechanism. *Nat Struct Mol Biol,* 17**,** 471-8.

Lee, M. E., T. A. Baker & R. T. Sauer (2010b) Control of substrate gating and translocation into ClpP by channel residues and ClpX binding. *J Mol Biol,* 399**,** 707-18.

Leung, E., A. Datti, M. Cossette, J. Goodreid, S. E. McCaw, M. Mah, A. Nakhamchik, K. Ogata, M. El Bakkouri, Y. Q. Cheng, S. J. Wodak, B. T. Eger, E. F. Pai, J. Liu, S. Gray-Owen, R. A. Batey & W. A. Houry (2011) Activators of cylindrical proteases as antimicrobials: identification and development of small molecule activators of ClpP protease. *Chem Biol,* 18**,** 1167-78.

Li, D. H., Y. S. Chung, M. Gloyd, E. Joseph, R. Ghirlando, G. D. Wright, Y. Q. Cheng, M. R. Maurizi, A. Guarne & J. Ortega (2010) Acyldepsipeptide antibiotics induce the formation of a structured axial channel in ClpP: A model for the ClpX/ClpA-bound state of ClpP. *Chem Biol,* 17**,** 959-69.

Licht, S. & I. Lee (2008) Resolving individual steps in the operation of ATP-dependent proteolytic molecular machines: from conformational changes to substrate translocation and processivity. *Biochemistry,* 47**,** 3595-605.

Martin, A., T. A. Baker & R. T. Sauer (2007) Distinct static and dynamic interactions control ATPase-peptidase communication in a AAA+ protease. *Mol Cell,* 27**,** 41-52.

Michel KH, Kastner RE. A54556 antibiotics and process for production thereof. US patent 4492650 1985**.**

Mindell, J. A. & N. Grigorieff (2003) Accurate determination of local defocus and specimen tilt in electron microscopy. *J Struct Biol,* 142**,** 334-47.

Nair, S., C. Poyart, J. L. Beretti, H. Veiga-Fernandes, P. Berche & P. Trieu-Cuot (2003) Role of the *Streptococcus agalactiae* ClpP serine protease in heat-induced stress defence and growth arrest. *Microbiology,* 149**,** 407-17.

Ortega, J., H. S. Lee, M. R. Maurizi & A. C. Steven (2002) Alternating translocation of protein substrates from both ends of ClpXP protease. *Embo J,* 21**,** 4938-49.

Ortega, J., S. K. Singh, T. Ishikawa, M. R. Maurizi & A. C. Steven (2000) Visualization of substrate binding and translocation by the ATP-dependent protease, ClpXP. *Mol Cell,* 6**,** 1515-21.

Penczek, P. A., R. A. Grassucci & J. Frank (1994) The ribosome at improved resolution: new techniques for merging and orientation refinement in 3D

cryo-electron microscopy of biological particles. *Ultramicroscopy,* 53**,** 251-70.

Pettersen, E. F., T. D. Goddard, C. C. Huang, G. S. Couch, D. M. Greenblatt, E. C. Meng & T. E. Ferrin (2004) UCSF Chimera--a visualization system for exploratory research and analysis. *J Comput Chem,* 25**,** 1605-12.

Rohrwild, M., O. Coux, H. C. Huang, R. P. Moerschell, S. J. Yoo, J. H. Seol, C. H. Chung & A. L. Goldberg (1996) HslV-HslU: A novel ATP-dependent protease complex in *Escherichia coli* related to the eukaryotic proteasome. *Proc Natl Acad Sci U S A,* 93**,** 5808-13.

Sass, P., M. Josten, K. Famulla, G. Schiffer, H. G. Sahl, L. Hamoen & H. Brotz-Oesterhelt (2011) Antibiotic acyldepsipeptides activate ClpP peptidase to degrade the cell division protein FtsZ. *Proc Natl Acad Sci U S A,* 108**,** 17474-9.

Sauer, R. T., D. N. Bolon, B. M. Burton, R. E. Burton, J. M. Flynn, R. A. Grant, G. L. Hersch, S. A. Joshi, J. A. Kenniston, I. Levchenko, S. B. Neher, E. S. Oakes, S. M. Siddiqui, D. A. Wah & T. A. Baker (2004) Sculpting the proteome with AAA(+) proteases and disassembly machines. *Cell,* 119**,** 9-18.

Schelin, J., F. Lindmark & A. K. Clarke (2002) The clpP multigene family for the ATP-dependent Clp protease in the cyanobacterium *Synechococcus*. *Microbiology,* 148**,** 2255-65.

Scheres, S. H., R. Nunez-Ramirez, C. O. Sorzano, J. M. Carazo & R. Marabini (2008) Image processing for electron microscopy single-particle analysis using XMIPP. *Nat Protoc,* 3**,** 977-90.

Schiefer, A., J. Vollmer, C. Lammer, S. Specht, C. Lentz, H. Ruebsamen-Schaeff, H. Brotz-Oesterhelt, A. Hoerauf & K. Pfarr (2013) The ClpP peptidase of *Wolbachia endobacteria* is a novel target for drug development against filarial infections. *J Antimicrob Chemother,* 68**,** 1790-800.

Singh, S. K., F. Guo & M. R. Maurizi (1999) ClpA and ClpP remain associated during multiple rounds of ATP-dependent protein degradation by ClpAP protease. *Biochemistry,* 38**,** 14906-15.

Singh, S. K., J. Rozycki, J. Ortega, T. Ishikawa, J. Lo, A. C. Steven & M. R. Maurizi (2001) Functional domains of the ClpA and ClpX molecular chaperones identified by limited proteolysis and deletion analysis. *J Biol Chem,* 276**,** 29420-9.

Sowole, M. A., J. A. Alexopoulos, Y. Q. Cheng, J. Ortega & L. Konermann (2013) Activation of ClpP protease by ADEP antibiotics: insights from hydrogen exchange mass spectrometry. *J Mol Biol,* 425**,** 4508-19.

Sprangers, R., A. Gribun, P. M. Hwang, W. A. Houry & L. E. Kay (2005) Quantitative NMR spectroscopy of supramolecular complexes: dynamic side pores in ClpP are important for product release. *Proc Natl Acad Sci U S A,* 102**,** 16678-83.

Thompson, M. W. & M. R. Maurizi (1994) Activity and specificity of *Escherichia coli* ClpAP protease in cleaving model peptide substrates. *J Biol Chem,* 269**,** 18201-8.

Thompson, M. W., S. K. Singh & M. R. Maurizi (1994) Processive degradation of proteins by the ATP-dependent Clp protease from *Escherichia coli*. Requirement for the multiple array of active sites in ClpP but not ATP hydrolysis. *J Biol Chem,* 269**,** 18209-15.

Vecchione, J. J. & J. K. Sello (2009) A novel tryptophanyl-tRNA synthetase gene confers high-level resistance to indolmycin. *Antimicrob Agents Chemother,* 53**,** 3972-80.

Viala, J., G. Rapoport & P. Mazodier (2000) The *clpP* multigenic family in *Streptomyces lividans*: conditional expression of the *clpP3 clpP4* operon is controlled by PopR, a novel transcriptional activator. *Mol Microbiol,* 38**,** 602-12.

Wang, J., J. A. Hartling & J. M. Flanagan (1997) The structure of ClpP at 2.3 A resolution suggests a model for ATP-dependent proteolysis. *Cell,* 91**,** 447-56.

Ye, F., J. Zhang, H. Liu, R. Hilgenfeld, R. Zhang, X. Kong, L. Li, J. Lu, X. Zhang, D. Li, H. Jiang, C. G. Yang & C. Luo (2013) Helix unfolding/refolding characterizes the functional dynamics of *Staphylococcus aureus* CLP protease. *J Biol Chem*.

Yoo, S. J., J. H. Seol, D. H. Shin, M. Rohrwild, M. S. Kang, K. Tanaka, A. L. Goldberg & C. H. Chung (1996) Purification and characterization of the heat shock proteins HslV and HslU that form a new ATP-dependent protease in *Escherichia coli*. *J Biol Chem,* 271**,** 14035-40.

Zhang, J., F. Ye, L. Lan, H. Jiang, C. Luo & C. G. Yang Structural switching of *Staphylococcus aureus* Clp protease: a key to understanding protease dynamics. *J Biol Chem,* 286**,** 37590-601.